12. Rubinsztein DC, Cuervo AM, Ravikumar B, Sarkar S, Korolchuk V, Kaushik S, Klionsky DJ. In search of an "autophagomometer". Autophagy 2009; 5:585-9.
13. Tanida I, Ueno T, Kominami E. LC3 and Autophagy. Methods Mol Biol 2008; 445:77-88.
14. Kabeya Y, Mizushima N, Ueno T, Yamamoto A, Kirisako T, Noda T, et al. LC3, a mammalian homologue of yeast Apg8p, is localized in autophagosome membranes after processing. EMBO J 2000; 19:5720-8.
15. Yamamoto A, Tagawa Y, Yoshimori T, Moriyama Y, Masaki R, Tashiro Y. Bafilomycin A1 prevents maturation of autophagic vacuoles by inhibiting fusion between autophagosomes and lysosomes in rat hepatoma cell line, H-4-II-E cells. Cell Struct Funct 1998; 23:33-42.
16. Mizushima N, Yoshimori T, Levine B. Methods in mammalian autophagy research. Cell 140:313-26.
17. Hanahan D, Weinberg RA. The hallmarks of cancer. Cell 2000; 100:57-70.
18. Ikenoue T, Hong S, Inoki K. Monitoring mammalian target of rapamycin (mTOR) activity. Methods Enzymol 2009; 452:165-80.
19. Sinn B, Tallen G, Schroeder G, Grassl B, Schulze J, Budach V, Tinhofer I. Caffeine confers radiosensitization of PTEN-deficient malignant glioma cells by enhancing ionizing radiation-induced G_1 arrest and negatively regulating Akt phosphorylation. Mol Cancer Ther 9:480-8.
20. Sarkaria JN, Busby EC, Tibbetts RS, Roos P, Taya Y, Karnitz LM, Abraham RT. Inhibition of ATM and ATR kinase activities by the radiosensitizing agent, caffeine. Cancer Res 1999; 59:4375-82.
21. Inoki K, Li Y, Xu T, Guan KL. Rheb GTPase is a direct target of TSC2 GAP activity and regulates mTOR signaling. Genes Dev 2003; 17:1829-34.
22. Inoki K, Li Y, Zhu T, Wu J, Guan KL. TSC2 is phosphorylated and inhibited by Akt and suppresses mTOR signalling. Nat Cell Biol 2002; 4:648-57.
23. Garami A, Zwartkruis FJ, Nobukuni T, Joaquin M, Roccio M, Stocker H, et al. Insulin activation of Rheb, a mediator of mTOR/S6K/4E-BP signaling, is inhibited by TSC1 and 2. Mol Cell 2003; 11:1457-66.
24. Muise-Helmericks RC, Grimes HL, Bellacosa A, Malstrom SE, Tsichlis PN, Rosen N. Cyclin D expression is controlled post-transcriptionally via a phosphatidylinositol-3-kinase/Akt-dependent pathway. J Biol Chem 1998; 273:29864-72.
25. Degtyarev M, De Maziere A, Orr C, Lin J, Lee BB, Tien JY, et al. Akt inhibition promotes autophagy and sensitizes PTEN-null tumors to lysosomotropic agents. J Cell Biol 2008; 183:101-16.
26. Wan X, Harkavy B, Shen N, Grohar P, Helman LJ. Rapamycin induces feedback activation of Akt signaling through an IGF-1R-dependent mechanism. Oncogene 2007; 26:1932-40.
27. Sun SY, Rosenberg LM, Wang X, Zhou Z, Yue P, Fu H, Khuri FR. Activation of Akt and eIF4E survival pathways by rapamycin-mediated mammalian target of rapamycin inhibition. Cancer Res 2005; 65:7052-8.
28. O'Reilly KE, Rojo F, She QB, Solit D, Mills GB, Smith D, et al. mTOR inhibition induces upstream receptor tyrosine kinase signaling and activates Akt. Cancer Res 2006; 66:1500-8.
29. Cirstea D, Hideshima T, Rodig S, Santo L, Pozzi S, Vallet S, et al. Dual inhibition of akt/mammalian target of rapamycin pathway by nanoparticle albumin-bound-rapamycin and perifosine induces antitumor activity in multiple myeloma. Mol Cancer Ther 2010; 9:963-75.
30. Aoki H, Takada Y, Kondo S, Sawaya R, Aggarwal BB, Kondo Y. Evidence that curcumin suppresses the growth of malignant gliomas in vitro and in vivo through induction of autophagy: role of Akt and extracellular signal-regulated kinase signaling pathways. Mol Pharmacol 2007; 72:29-39.
31. Ellington AA, Berhow MA, Singletary KW. Inhibition of Akt signaling and enhanced ERK1/2 activity are involved in induction of macroautophagy by triterpenoid B-group soyasaponins in colon cancer cells. Carcinogenesis 2006; 27:298-306.
32. Rubinsztein DC, Gestwicki JE, Murphy LO, Klionsky DJ. Potential therapeutic applications of autophagy. Nat Rev Drug Discov 2007; 6:304-12.
33. Ravikumar B, Vacher C, Berger Z, Davies JE, Luo S, Oroz LG, et al. Inhibition of mTOR induces autophagy and reduces toxicity of polyglutamine expansions in fly and mouse models of Huntington disease. Nat Genet 2004; 36:585-95.
34. Kotake Y, Ohta S. MPP^+ analogs acting on mitochondria and inducing neuro-degeneration. Curr Med Chem 2003; 10:2507-16.
35. Hagan MP, Hopcia KL, Sylvester FC, Held KD. Caffeine-induced apoptosis reveals a persistent lesion after treatment with bromodeoxyuridine and ultraviolet-B light. Radiat Res 1997; 147:674-9.
36. Efferth T, Fabry U, Glatte P, Osieka R. Expression of apoptosis-related oncoproteins and modulation of apoptosis by caffeine in human leukemic cells. J Cancer Res Clin Oncol 1995; 121:648-56.
37. Shinomiya N, Takemura T, Iwamoto K, Rokutanda M. Caffeine induces S-phase apoptosis in cis-diamminedichloroplatinum-treated cells, whereas cis-diamminedichloroplatinum induces a block in G_2/M. Cytometry 1997; 27:365-73.
38. Lau CC, Pardee AB. Mechanism by which caffeine potentiates lethality of nitrogen mustard. Proc Natl Acad Sci USA 1982; 79:2942-6.
39. Takagi M, Shigeta T, Asada M, Iwata S, Nakazawa S, Kanke Y, et al. DNA damage-associated cell cycle and cell death control is differentially modulated by caffeine in clones with p53 mutations. Leukemia 1999; 13:70-7.
40. Ormerod MG, Collins MK, Rodriguez-Tarduchy G, Robertson D. Apoptosis in interleukin-3-dependent haemopoietic cells. Quantification by two flow cytometric methods. J Immunol Methods 1992; 153:57-65.
41. Kawatani M, Uchi M, Simizu S, Osada H, Imoto M. Transmembrane domain of Bcl-2 is required for inhibition of ceramide synthesis, but not cytochrome *c* release in the pathway of inostamycin-induced apoptosis. Exp Cell Res 2003; 286:57-66.
42. Kawajiri S, Saiki S, Sato S, Sato F, Hatano T, Eguchi H, Hattori N. PINK1 is recruited to mitochondria with parkin and associates with LC3 in mitophagy. FEBS Lett 2010; 584:1073-9.
43. Sarkar S, Davies JE, Huang Z, Tunnacliffe A, Rubinsztein DC. Trehalose, a novel mTOR-independent autophagy enhancer, accelerates the clearance of mutant huntingtin and alpha-synuclein. J Biol Chem 2007; 282:5641-52.

Neurobiology of Disease 41 (2011) 111–118

Contents lists available at ScienceDirect

Neurobiology of Disease

journal homepage: www.elsevier.com/locate/ynbdi

Mitochondrial membrane potential decrease caused by loss of PINK1 is not due to proton leak, but to respiratory chain defects

Taku Amo [a,1], Shigeto Sato [b], Shinji Saiki [b], Alexander M. Wolf [a], Masaaki Toyomizu [c], Clement A. Gautier [d], Jie Shen [d], Shigeo Ohta [a], Nobutaka Hattori [b,*]

[a] Department of Biochemistry and Cell Biology, Institute of Development and Aging Sciences, Graduate School of Medicine, Nippon Medical School, 1-396 Kosugi-cho, Nakahara-ku, Kawasaki 211-8533, Japan
[b] Department of Neurology, Juntendo University School of Medicine, 2-1-1 Hongo, Bunkyo-ku, Tokyo 113-8421, Japan
[c] Animal Nutrition, Life Sciences, Graduate School of Agricultural Science, Tohoku University, 1-1 Tsutsumidori-Amamiyamachi, Aoba-ku, Sendai 981-8555, Japan
[d] Center for Neurologic Diseases, Brigham and Women's Hospital, Program in Neuroscience, Harvard Medical School, Boston, MA 02115, USA

ARTICLE INFO

Article history:
Received 29 June 2010
Revised 17 August 2010
Accepted 25 August 2010
Available online 15 September 2010

Keywords:
Parkinson's disease
Mitochondria
PINK1
Parkin
Membrane potential
Oxidative phosphorylation
Modular kinetic analysis
Proton leak
Reactive oxygen species

ABSTRACT

Mutations in *PTEN-induced putative kinase 1* (*PINK1*) cause a recessive form of Parkinson's disease (PD). PINK1 is associated with mitochondrial quality control and its partial knock-down induces mitochondrial dysfunction including decreased membrane potential and increased vulnerability against mitochondrial toxins, but the exact function of PINK1 in mitochondria has not been investigated using cells with null expression of PINK1. Here, we show that loss of PINK1 caused mitochondrial dysfunction. In PINK1-deficient ($PINK1^{-/-}$) mouse embryonic fibroblasts (MEFs), mitochondrial membrane potential and cellular ATP levels were decreased compared with those in littermate wild-type MEFs. However, mitochondrial proton leak, which reduces membrane potential in the absence of ATP synthesis, was not altered by loss of PINK1. Instead, activity of the respiratory chain, which produces the membrane potential by oxidizing substrates using oxygen, declined. H_2O_2 production rate by $PINK1^{-/-}$ mitochondria was lower than $PINK1^{+/+}$ mitochondria as a consequence of decreased oxygen consumption rate, while the proportion (H_2O_2 production rate per oxygen consumption rate) was higher. These results suggest that mitochondrial dysfunctions in PD pathogenesis are caused not by proton leak, but by respiratory chain defects.

© 2010 Elsevier Inc. All rights reserved.

Introduction

Parkinson's disease (PD) is a neurodegenerative disease characterized by loss of dopaminergic neurons in the substantia nigra. Mitochondrial dysfunction has been proposed as a major factor in the pathogenesis of sporadic and familial PD (Abou-Sleiman et al., 2006). In particular, the identification of mutations in *PTEN-induced putative kinase 1* (*PINK1*) has strongly implicated mitochondrial dysfunction owing to its loss of function in the pathogenesis of PD (Valente et al., 2004). PINK1 contains an N-terminal mitochondrial targeting sequence (MTS) and a serine/threonine kinase domain (Valente et al., 2004). PINK1 kinase activity is crucial for mitochondrial maintenance via TRAP phosphorylation (Pridgeon et al., 2007). Loss of PINK1 function induces increased vulnerability to various stresses (Exner et al., 2007; Haque et al., 2008; Pridgeon et al., 2007; Wood-Kaczmar et al., 2008). However, silencing of PINK1 has only been partial and only one study has been performed to assess mitochondrial functions in steady and artificial states with complete ablation of PINK1 expression (Gautier et al., 2008).

Several studies have shown that PINK1 acts upstream of parkin in the same genetic pathway (Clark et al., 2006; Park et al., 2006) and co-overexpressed PINK1 and parkin both co-localized to mitochondria (Kim et al., 2008). Overexpression of PINK1 promotes mitochondrial fission (Yang et al., 2008). Fission followed by selective fusion segregates dysfunctional mitochondria and permits their removal by autophagy (Twig et al., 2008). PINK1 loss-of-function decreases mitochondrial membrane potential (Chu, 2010) and the PINK1–parkin pathway is associated with mitochondrial elimination in cultured cells treated with the mitochondrial uncoupler carbonyl cyanide *m*-chlorophenylhydrazone (CCCP), which causes mitochondrial depolarization (Geisler et al., 2010; Kawajiri et al., 2010; Matsuda et al., 2010; Narendra et al., 2008, 2010; Vives-Bauza et al., 2010). However, the exact mechanism underlying the mitochondrial depolarization induced by PINK1 defects leading to mitochondrial autophagy has not been examined in detail.

Abbreviations: $\Delta\psi$, mitochondrial membrane potential; FCCP, carbonyl cyanide *p*-trifluoromethoxyphenylhydrazone; MEFs, mouse embryonic fibroblasts; PD, Parkinson's disease; PINK1, PTEN-induced putative kinase 1; ROS, reactive oxygen species; TMRM, tetramethylrhodamine methyl ester; TPMP, triphenylmethylphosphonium.

* Corresponding author. Fax: +81 3 5800 0547.
E-mail address: nhattori@juntendo.ac.jp (N. Hattori).
[1] Present address: Department of Applied Chemistry, National Defense Academy, 1-10-20 Hashirimizu, Yokosuka 239-8686, Japan.

Available online on ScienceDirect (www.sciencedirect.com).

0969-9961/$ – see front matter © 2010 Elsevier Inc. All rights reserved.
doi:10.1016/j.nbd.2010.08.027

Here, we describe a detailed characterization of mitochondria in PINK1-deficient cells. We show that PINK1 deficiency causes a decrease in mitochondrial membrane potential, which is not due to proton leak, but to respiratory chain defects.

Materials and methods

PINK1 knock-out mouse embryonic fibroblasts (MEFs)

PINK1 knock-out MEFs were prepared and cultured as described previously (Matsuda et al., 2010). Mouse embryonic fibroblasts (MEFs) were derived from E12.5 embryos containing littermate 4 mice of each genotype. Embryos were mechanically dispersed by repeated passage through a P1000 pipette tip and plated with MEF media containing DME, 10% FCS, 1× nonessential amino acids, 1 mM L-glutamine, penicillin/streptomycin (invitrogen). The $\psi 2$ cell line, an ecotropic retrovirus packaging cell line, was maintained in Dulbecco's modified Eagle medium (DMEM, Sigma) with 5% fetal bovine serum and 50 μg/ml kanamicin. Transfection of the $\psi 2$ cells with pMESVTS plasmids containing an SV40 large T antigen was performed by lipofection method according to the manual provided by the manufacturer (GIBCO BRL). Five micrograms of the plasmids was used for each transfection. Transfectants were selected by G418 at the concentration of 0.5 mg/ml, and 10 clonal cell lines were established. The highest titer of 5×10^4 cfu/ml was obtained for the conditioned medium of a cell line designated ψ2SVTS1. 10^6 MEFs were plated onto a 10-cm culture dish and kept at 33 °C for 48 hours. Then medium was replaced with 2 ml supplemented with polybrene-supplemented medium conditioned by the ψ2SVTS1 cells at confluency for 3 days. Infection was continued for 3 hours, and the medium was replaced with a fresh one. The infected MEFs were cultured at 33 °C until immortalized cells were obtained.

We confirmed that the differences we detected in this study were due to the PINK1 deficiency, not to artificial effects by immortalization, by measuring cellular respiration rates of not immortalized MEFs from other littermates (Supplemental figure). The respiration rates of not immortalized MEFs were slightly slower than those of immortalized MEFs, but the differences between PINK1$^{+/+}$ and $^{-/-}$ MEFs were consistent (Fig. 2A).

Cell growth

Cells were seeded in 12-well plates at density of $3\sim6 \times 10^3$ cells/well and incubated in DMEM high glucose medium (4.5 g/l glucose and 1 mM sodium pyruvate) supplemented with 10% fetal bovine serum. After a day, the medium was replaced with DMEM glucose-free medium supplemented with 1 g/l galactose, 1 mM sodium pyruvate and 10% fetal bovine serum (DMEM galactose medium) at 37 °C in an incubator with a humidified atmosphere of 5% CO_2. Cells were trypsinized and live cells were assessed by trypan blue dye exclusion.

Mitochondrial morphological changes

Cells were seeded in 6-well plates at 2.0×10^5/well and incubated in DMEM high glucose medium (4.5 g/l glucose and 1 mM sodium pyruvate) supplemented with 10% fetal bovine serum and 1% penicillin/streptomycin. After a day, the medium was replaced with DMEM glucose-free medium supplemented with 1 g/l galactose, 1 mM sodium pyruvate and 10% fetal bovine serum (DMEM galactose medium) at 37 °C in an incubator with a humidified atmosphere of 5% CO_2. 24 hours later, cells were fixed and immunostained with anti-Tom20 antibody to visualize mitochondria according to a protocol as previously described (Kawajiri et al., 2010). All images were obtained using an Axioplan 2 imaging microscope (Carl Zeiss, Oberkochen, Germany).

Cellular ATP levels

Intracellular ATP levels were determined by a cellular ATP assay kit (TOYO B-Net, Tokyo, Japan) according to the manufacturer's instructions using a Lumat LB9507 luminometer (Berthold Technology, Bad Wildbad, Germany).

Membrane potential

Fluorescence images were recorded using a multi-dimensional imaging workstation (AS MDW, Leica Microsystems, Wetzlar, Germany) with a climate chamber maintained at 37 °C. Fluorescence was quantified with a CCD camera (CoolSnap HQ, Roper Scientific, Princeton, NJ) using a 20× objective. Cells were stained for 1 hour with a non-quenching concentration (20 nM) of tetramethylrhodamine methyl ester (TMRM) in a 96-well plate. The cell-permeable cationic dye TMRM accumulates in mitochondria according to the Nernst equation. Nuclei were stained with 250 nM Hoechst 34580. Mitochondrial TMRM fluorescence was integrated in a 40-μm diameter circular area around the nucleus, and the minimum fluorescence in this area was subtracted as background fluorescence.

Cell respiration

Cell respiration was measured at 37 °C using the Oxygen Meter Model 781 and the Mitocell MT200 closed respiratory chamber (Strathkelvin Instruments, North Lanarkshire, United Kingdom). Cells were cultured in DMEM with 4.5 g/l of glucose supplemented with 10% FBS. Cells were then trypsinized and resuspended in Leibovitz's L-15 medium (Invitrogen) at density of 8.0×10^6 cells/ml. The oxygen respiration rate was measured under each of the following three conditions: basal rate (no additions); State 4 (no ATP synthesis) [after addition of 1 μg/ml oligomycin (Sigma)], uncoupled [after addition of 3 μM FCCP (carbonyl cyanide *p*-trifluoromethoxyphenylhydrazone; Sigma)] using Strathkelvin 949 Oxygen System. After sequential measurements, the endogenous respiration rate was determined by adding 1 μM rotenone + 2 μM myxothiazol.

Mitochondrial respiration and membrane potential

Mitochondria were prepared from cultured MEFs as previously described (Amo and Brand, 2007). Mitochondrial oxygen consumption with 5 mM succinate as a respiratory substrate was measured at 37 °C using a Clark electrode (Rank Brothers, Cambridge, United Kingdom) calibrated with air-saturated respiration buffer comprising 0.115 M KCl, 10 mM KH_2PO_4, 3 mM HEPES (pH 7.2), 2 mM $MgCl_2$, 1 mM EGTA and 0.3% (w/v) defatted BSA, assumed to contain 406 nmol atomic oxygen/ml (Reynafarje et al., 1985). Mitochondrial membrane potential ($\Delta\psi$) was measured simultaneously with respiratory activity using an electrode sensitive to the lipophilic cation $TPMP^+$ (triphenylmethylphosphonium) (Brand, 1995). Mitochondria were incubated at 0.5 mg/ml in the presence of 80 ng/ml nigericin (to collapse the pH gradient so that the proton motive force was expressed exclusively as $\Delta\psi$) and 2 μM rotenone (to inhibit complex I). The $TPMP^+$-sensitive electrode was calibrated with sequential additions of $TPMP^+$ up to 2 μM, then 5 mM succinate was added to initiate respiration. Experiments were terminated with 2 μM FCCP, allowing correction for any small baseline drift. $\Delta\psi$ was calculated from the distribution of $TPMP^+$ across the mitochondrial inner membrane using a binding correction factor of 0.35 mg protein/μl. Respiratory rates with 4 mM pyruvate + 1 mM malate as a substrate in State 3 (with 0.25 mM ADP) and State 4 (with 1 μg/ml oligomycin) were determined using the Oxygen Meter Model 781 and the Mitocell MT200 closed respiratory chamber (Strathkelvin Instruments).

Modular kinetic analysis

To investigate differences in oxidative phosphorylation caused by PINK1 knock-out, we applied a systems approach, namely modular kinetic analysis (Amo and Brand, 2007; Brand, 1990). This analyzes the kinetics of the whole of oxidative phosphorylation divided into three modules connected by their common substrate or product, $\Delta\psi$. The modules are (i) the reactions that produce $\Delta\psi$, consisting of the substrate translocases, dehydrogenases and other enzymes and the components of the respiratory chain, called 'substrate oxidation'; (ii) the reactions that consume $\Delta\psi$ and synthesize, export and dephosphorylate ATP, consisting of ATP synthase, the phosphate and adenine nucleotide translocases and any ATPases that may be present, called the 'phosphorylating system'; and (iii) the reactions that consume $\Delta\psi$ without ATP synthesis, called the 'proton leak' (Brand, 1990). The analysis reports changes anywhere within oxidative phosphorylation that are functionally important but is unresponsive to changes that have no functional consequences. Comparison of the kinetic responses of each of the three modules to $\Delta\psi$ obtained using mitochondria isolated from PINK1$^{+/+}$ and PINK1$^{-/-}$ MEFs would reveal any effects of PINK1 on the kinetics of oxidative phosphorylation. Oxygen consumption and $\Delta\psi$ were measured simultaneously using mitochondria incubated with 80 ng/ml nigericin and 4 μM rotenone. Respiration was initiated by 5 mM succinate. The kinetic behavior of a '$\Delta\psi$-producer' can be established by specific modulation of a $\Delta\psi$-consumer and the kinetics of a consumer can be established by specific modulation of a $\Delta\psi$-producer (Brand, 1998). To measure the kinetic response of proton leak to $\Delta\psi$, the State 4 (non-phosphorylating) respiration of mitochondria in the presence of oligomycin (0.8 μg/ml; to prevent any residual ATP synthesis), which was used solely to drive the proton leak, was titrated with malonate (up to 8 mM). In a similar way, State 4 respiration was titrated by FCCP (up to 1 μM) for measurement of the kinetic response of substrate oxidation to $\Delta\psi$. State 3 (maximal rate of ATP synthesis) was obtained by addition of excess ADP (1 mM). Titration of State 3 respiration with malonate (up to 1.1 mM) allowed measurement of the kinetics of the $\Delta\psi$-consumers (the sum of the phosphorylating system and proton leak). The coupling efficiencies of oxidative phosphorylation were calculated from the kinetic curves as the percentage of mitochondrial respiration rate at a given $\Delta\psi$ that was used for ATP synthesis and was therefore inhibited by oligomycin. Note that any slip reactions will appear as proton leak in this analysis (Brand et al., 1994).

Mitochondrial ROS production

Mitochondrial ROS production rate was assessed by measurement of H_2O_2 generation rate, determined fluorometrically by measurement of oxidation of Amplex Red to fluorescent resorufin coupled to the enzymatic reduction of H_2O_2 by horseradish peroxidase using a spectrofluorometer RF-5300PC (Shimadzu, Kyoto, Japan). The H_2O_2 generation rate was measured in non-phosphorylating conditions (=State 4) using either pyruvate/malate or succinate as respiratory substrates. Mitochondria were incubated at 0.1 mg/ml in respiration buffer. All incubations also contained 5 μM Amplex Red, 2 U/ml horseradish peroxidase and 8 U/ml superoxide dismutase. The reaction was initiated by addition of 5 mM succinate or 4 mM pyruvate + 1 mM malonate and the increase in fluorescence was followed at excitation and emission wavelengths of 560 and 590 nm, respectively. Appropriate correction for background signals and standard curves generated using known amounts of H_2O_2 were used to calculate the rate of H_2O_2 production in nmol/min/mg mitochondrial protein. The percentage free radical leak, which is a measure of the number of electrons that produce superoxide (and subsequently H_2O_2) compared with the total number of electrons which pass thorough the respiratory chain, was calculated as the rate of H_2O_2 production divided by the rate of O_2 consumption (Barja et al., 1994).

Statistics

Values are presented as means ± SEM except Fig. 2D, in which error bars indicate SD. The significance of differences between means was assessed by the unpaired Student's *t*-test using Microsoft Excel; *P* values < 0.05 were taken to be significant.

Results

Cell growth and mitochondrial morphology

In general, cultured cells gain their energy mostly from glycolysis. Therefore, cells deficient in respiratory function can grow in normal medium, although possibly at a slower rate, relying predominantly on glycolysis (Hofhaus et al., 1996). Actually, ρ^0 cells, which lack mitochondrial DNA completely, can grow producing energy exclusively through glycolysis (King and Attardi, 1989). On the other hand, galactose metabolism via glycolysis is much slower than glucose metabolism (Reitzer et al., 1979). Therefore, cells in galactose medium are forced to oxidize pyruvate through the mitochondrial respiratory chain for energy required for growth. Consequently, cells with defects in their mitochondrial respiratory chains show growth impairments in galactose medium. To evaluate this phenomenon is also observed in our cells, we examined growth retardation by addition of mitochondrial complex I inhibitor, rotenone (Fig. 1A). In glucose medium, 10 nM rotenone had only a slight effect on the growth of PINK1$^{+/+}$ MEFs and slower growth was observed even in the presence of 100 nM rotenone. However, in the galactose medium, 10 nM rotenone significantly inhibited the growth of PINK1$^{+/+}$ MEFs and 100 nM roteone completely arrested the growth. Therefore, we could confirm that the growth impairment of our cells in the galactose medium was due to mitochondrial respiratory chain defects.

PINK1 acts upstream of parkin, regulating mitochondrial integrity and function; therefore, loss of PINK1 is considered to affect mitochondrial functions. To assess the mitochondrial functions of PINK1$^{-/-}$ MEFs, growth capability in a medium in which galactose replaced glucose was examined. As shown in Fig. 1B, PINK1$^{-/-}$ MEFs appeared to show clear growth impairments in the galactose medium, whereas PINK1$^{+/+}$ MEFs grew slightly slower than in the glucose medium.

No differences of mitochondrial morphology between PINK1$^{+/+}$ and $^{-/-}$ MEFs in the glucose medium were detected (Fig. 1C), consistent with the previous report (Matsuda et al., 2010). However, in the galactose medium, mitochondria of the PINK1$^{-/-}$ MEFs were more fragmented compared to the PINK$^{+/+}$ MEFs (Fig. 1C). This is consistent with previous reports, which found mitochondrial morphological changes were more pronounced when PINK1 knock-down HeLa cells were grown in low-glucose medium (Exner et al., 2007) and human PINK1 homozygous mutant fibroblast in galactose medium (Grünewald et al., 2009). In these cells, mitochondrial morphological changes were associated with the mitochondrial functional impairment.

Assessments of mitochondrial functions at the cellular level

Because PINK1$^{-/-}$ MEFs showed severe growth impairments in the galactose medium, the mitochondrial functions of these cells were assessed at the cellular level. First, cellular respiration rates were measured (Fig. 2A). The basal respiration rate was significantly reduced in PINK1$^{-/-}$ cells compared with that in PINK1$^{+/+}$ cells (11.13 ± 0.71 versus 14.36 ± 1.01 nmol O/min/10^6 cells; $p < 0.05$; $n = 5$ independent experiments), consistent with previous reports using partial knock-down of PINK1 expression (Gandhi et al., 2009; Liu et al., 2009). Oligomycin inhibits ATP synthase, resulting in non-phosphorylating respiration. FCCP uncouples oxidative phosphorylation, leading to maximum respiration rates. In both conditions, the

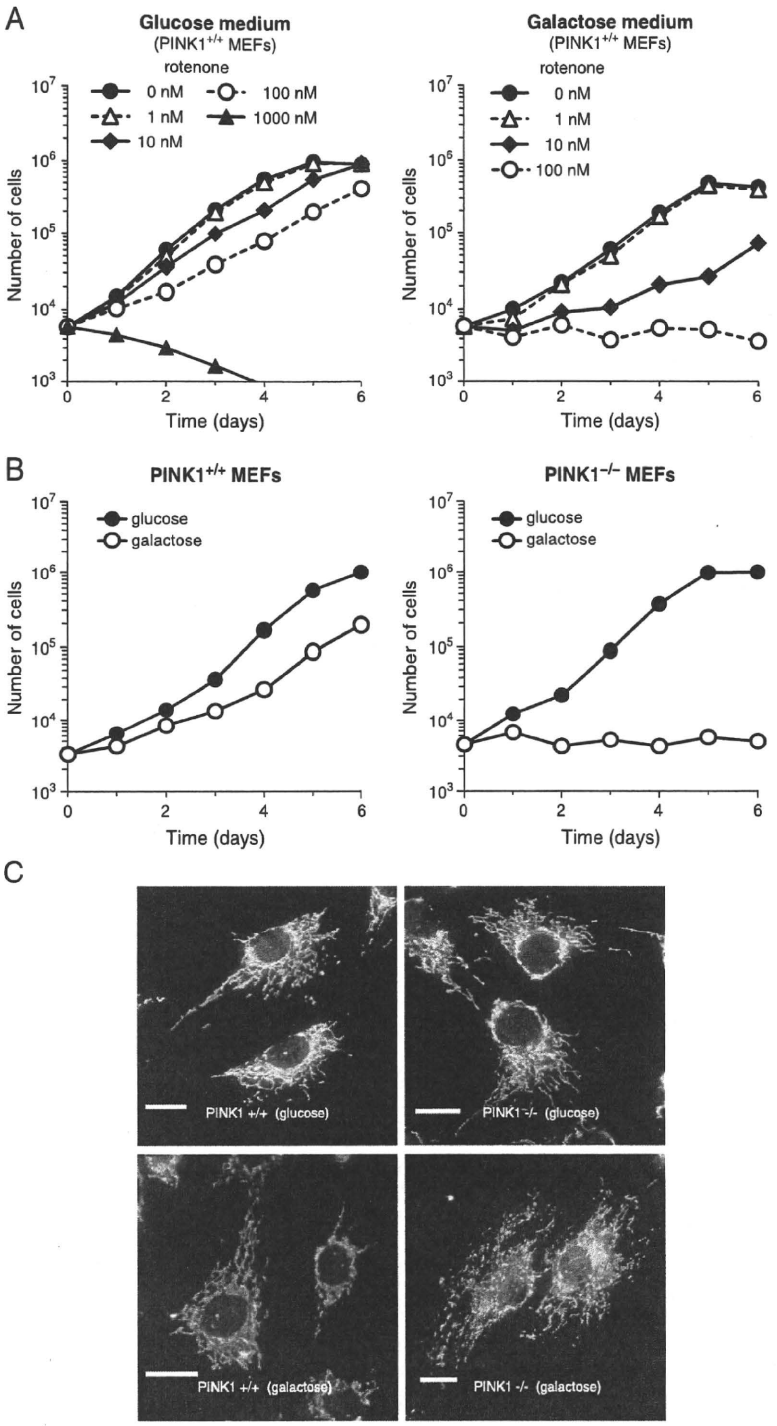

Fig. 1. (A) Growth retardation of PINK1$^{+/+}$ MEFs by mitochondrial complex I inhibitor, rotenone in glucose or galactose medium. Closed circles with solid line, 0 nM rotenone; open triangles with dashed line, 1 nM rotenone; closed diamonds with solid line, 10 nM rotenone; open circles with dashed line, 100 nM rotenone; closed triangles with solid line, 1000 nM rotenone. Cells grown in 12-well plates were trypsinized and live cells were assessed by trypan blue dye exclusion. (B) Growth curves of PINK1$^{+/+}$ and $^{-/-}$ MEFs. Closed symbols (*glucose*), growth curve for cells grown in DMEM containing 4.5 g/l glucose and 1 mM sodium pyruvate; open symbols (*galactose*), growth curve for cells grown in DMEM lacking glucose and containing instead 1.0 g/l galactose and 1 mM sodium pyruvate. Cells grown in 12-well plates were trypsinized and live cells were assessed by trypan blue dye exclusion. (C) Mitochondrial morphology of PINK1$^{+/+}$ and $^{-/-}$ MEFs. After incubating cells with the glucose or galactose medium for 24 hours, cells were fixed and immunostained with anti-Tom20 antibody to visualize mitochondria. Scale bar, 20 μm.

PINK1$^{-/-}$ cells respired significantly slower than the PINK1$^{+/+}$ cells (1.76 ± 0.13 versus 2.95 ± 0.27 ($p<0.01$; $n=5$ independent experiments) and 16.44 ± 1.80 versus 23.50 ± 1.18 nmol O/min/10^6 cells ($p<0.05$; $n=5$ independent experiments), respectively).

The main function of mitochondria is ATP synthesis via oxidative phosphorylation. ATP levels under basal conditions were significantly reduced in PINK1$^{-/-}$ MEFs (Fig. 2B), as reported previously for dissociated PINK1$^{-/-}$ mouse neurons (Gispert et al., 2009) and PINK1

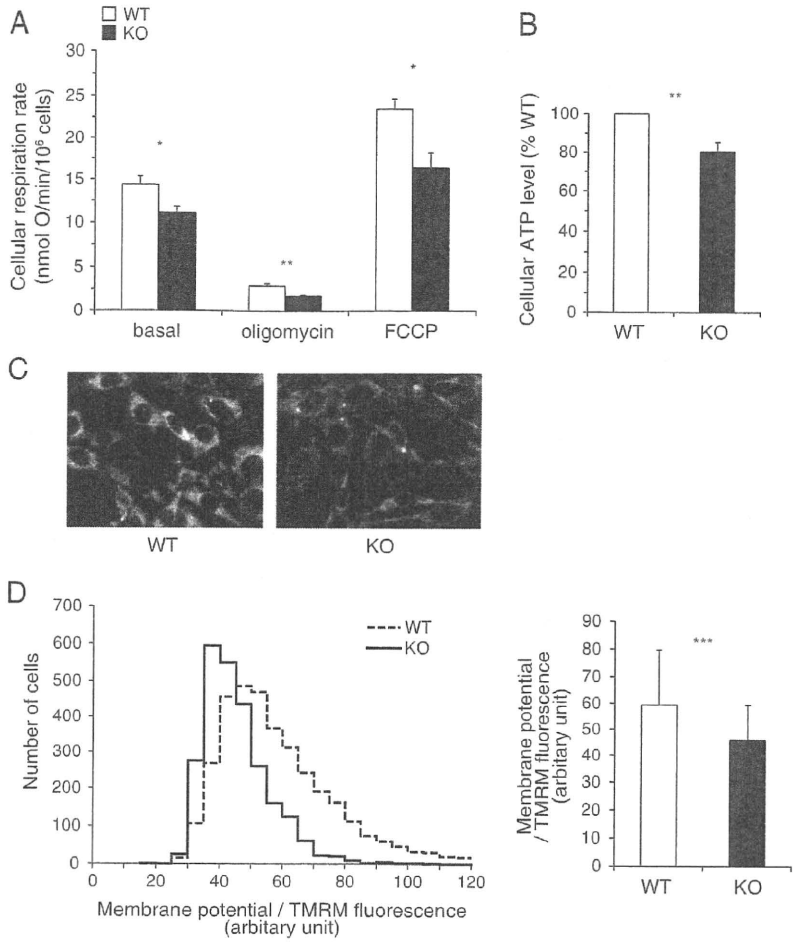

Fig. 2. Mitochondrial functions assessed at the cellular level. Open bars, PINK1 $^{+/+}$ MEFs; closed bars, PINK1 $^{-/-}$ MEFs. (A) Cell respiration rate of PINK1 $^{+/+}$ and $^{-/-}$ MEFs. The oxygen respiration rate was measured at density of 8.0×10^6 cells/ml under each of the following three conditions: basal rate (no additions); State 4 (no ATP synthesis) [after addition of 1 μg/ml oligomycin], uncoupled [after addition of 3 μM FCCP]. After sequential measurements, the endogenous respiration rate was determined by adding 1 μM rotenone + 2 μM myxothiazol. Error bars indicate SEM ($n = 5$ independent experiments). (B) Cellular ATP levels. Data were normalized based on cell numbers and expressed as the percentage of the level in PINK1 $^{+/+}$ cells. Error bars indicate SEM ($n = 4$ independent experiments). (C) Live cell images of PINK1 $^{+/+}$ and $^{-/-}$ MEFs with TMRM fluorescence. (D) Mitochondrial membrane potential evaluated by live cell imaging of TMRM fluorescence. *Left panel*, the distribution of TMRM fluorescence from 3537 PINK1 $^{+/+}$ and 2566 PINK1 $^{-/-}$ cells from 12 wells per cell type; *right panel*, the average value of TMRM fluorescence per cell. Error bars indicate SD. $^{*}P<0.05$; $^{**}P<0.01$; $^{***}P<0.001$.

siRNA knock-down PC12 cells (Liu et al., 2009). Mitochondrial membrane potential was also measured by live cell imaging of TMRM fluorescence. Typical images were shown in Fig. 2C. The histogram shows the distribution of TMRM fluorescence from 3537 PINK1 $^{+/+}$ cells and 2566 PINK1 $^{-/-}$ cells from 12 wells per cell type and the bar graph indicates the mean ± SD of TMRM fluorescence per cell (Fig. 2D). According to the Nernst equation, the ratio of TMRM fluorescence would translate into, on average, 6.88 mV lower mitochondrial membrane potential in the PINK1 $^{-/-}$ cells if the plasma membrane potentials were not different between PINK1 $^{+/+}$ and $^{-/-}$ cells. Mitochondrial membrane potential decrease was also showed previously in PINK1 knock-down HeLa cells (Exner et al., 2007) and in stable PINK1 knock-down neuroblastoma cell lines (Sandebring et al., 2009).

Assessments of mitochondrial functions using isolated mitochondria

To further analyze mitochondrial functions, we measured the kinetics of oxidative phosphorylation using isolated mitochondria from PINK1 $^{+/+}$ and $^{-/-}$ MEFs. Fig. 3 shows the kinetics of the three modules of oxidative phosphorylation using succinate as a respiratory substrate (complex II-linked respiration). Fig. 3A shows the kinetic response of substrate oxidation to its product, $\Delta\psi$. The substrate oxidation kinetic curve for PINK1 $^{-/-}$ cells was clearly shifted lower compared with that for PINK1 $^{+/+}$ cells, indicating that the loss of PINK1 caused mitochondrial respiratory chain defects. Fig. 3B shows the kinetic response of proton leak to its driving force, $\Delta\psi$, and Fig. 3C shows the kinetic response of the ATP phosphorylating pathway to its driving force, $\Delta\psi$. Both kinetic curves for PINK1 $^{+/+}$ and $^{-/-}$ MEFs (open and closed symbols, respectively) were overlapping, implying that there were no significant differences in those modules.

We also independently measured the mitochondrial oxygen consumption rate using pyruvate/malate as a respiratory substrate instead of succinate to check complex I. Modular kinetic analysis using pyruvate/malate is technically difficult for the following reasons: (1) the oxygen consumption rate with pyruvate/malate is much slower than succinate respiration; and (2) there are no competitive inhibitors of complex I-linked respiration, such as malonate for succinate respiration. As shown in Fig. 4A, the respiration rates in State 3 and 4 with pyruvate/malate of isolated mitochondria from PINK1 $^{-/-}$ cells (closed symbols) were significantly slower than those of PINK1 $^{+/+}$ cells (open symbols), as in the case of succinate respiration (Fig. 4B; data derived from the kinetic curves in Fig. 3).

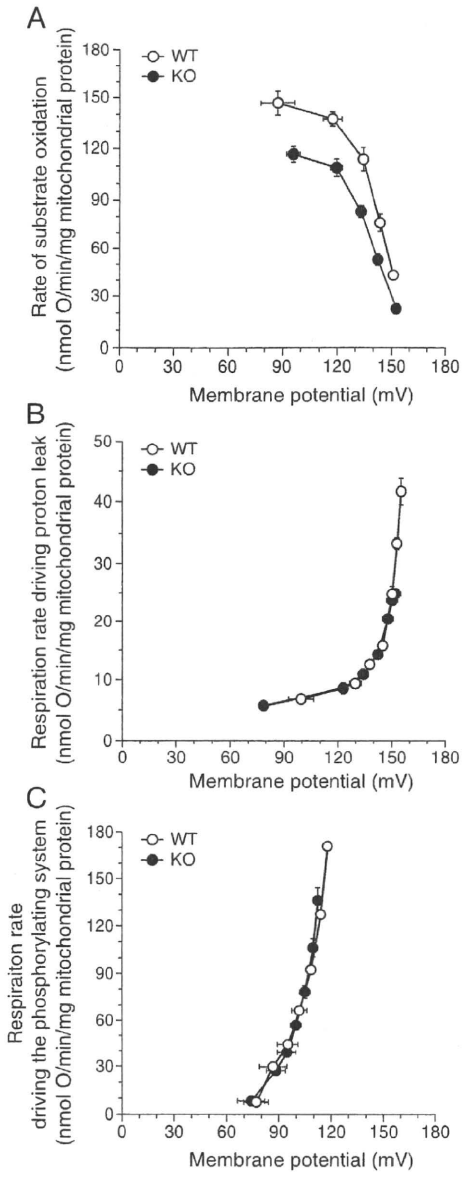

Fig. 3. Modular kinetic analysis of oxidative phosphorylation in mitochondria isolated from PINK1$^{+/+}$ and $^{-/-}$ MEFs. Modular kinetic analysis of the kinetic responses to membrane potential, $\Delta\psi$, of respiration driving (A) substrate oxidation ($\Delta\psi$ titrated with uncoupler, FCCP, starting in State 4), (B) proton leak ($\Delta\psi$ titrated with malonate, starting in State 4) and (C) the phosphorylating system, calculated by subtracting respiration driving proton leak from respiration driving the $\Delta\psi$-consumers ($\Delta\psi$ titrated with malonate starting in State 3; not shown) at each $\Delta\psi$. Open symbols, PINK1$^{+/+}$ MEFs; closed symbols, PINK1$^{-/-}$ MEFs. Error bars indicate SEM ($n=4$ independent mitochondrial preparations).

Mitochondrial ROS production

Mitochondrial ROS production rate was assessed by measurement of the H_2O_2 generation rate. Mechanisms of mitochondrial ROS production were well described elsewhere (Fig. 1 of Lambert et al., 2010). Pyruvate and malate generate NADH, which induced forward electron transport and generate ROS mainly from complex I and III. For pyruvate/malate respiration, the basal H_2O_2 generation rate (measured in the absence of respiratory chain inhibitors) was not different between PINK1$^{+/+}$ and $^{-/-}$ mitochondria (Fig. 4C). The addition of antimycin A and further addition of rotenone, which inhibited forward electron transport at complex III and I, respectively, enhanced H_2O_2 generation. During succinate respiration in the absence of respiratory chain inhibitors, ROS are generated mainly from the quinine binding site of complex I due to reverse electron flow from coenzyme Q to complex I. For succinate respiration, H_2O_2 generation rate in the absence of reparatory chain inhibitors was higher in PINK1$^{+/+}$ mitochondria than in PINK1$^{-/-}$ mitochondria, but the difference was not significant (Fig. 4D). The addition of rotenone, which blocks reverse electron flow from coenzyme Q to complex I, attenuated H_2O_2 generation.

Figs. 4 C and D show a tendency for PINK1$^{+/+}$ mitochondria to generate more ROS than PINK1$^{-/-}$ mitochondria. However, their respiration rates were remarkably different (Figs. 4A and B). Therefore, we calculated the percentage free radical leak, which is the fraction of molecules of O_2 consumed that give rise to H_2O_2 release by mitochondria (free radical leak) during either pyruvate/malate or succinate State 4 respiration (Figs. 4E and F). For pyruvate/malate respiration, mitochondria isolated from PINK1$^{-/-}$ cells had higher proportion of H_2O_2 generation than PINK1$^{+/+}$ mitochondria. During succinate respiration without respiratory inhibitors, PINK1$^{-/-}$ mitochondria had also higher proportion of free radical leak mainly from complex I due to reverse electron flow from coenzyme Q to complex I. Because the differences disappeared with addition of rotenone, which inhibit reverse electron flow, ROS generation enhanced by loss of PINK1 was mostly from complex I.

Discussion

We produced an *in vitro* model of Parkinson's disease, immortalized PINK1$^{-/-}$ MEFs. Previously, impairment of mitochondrial respiration was observed in the brains of PINK1$^{-/-}$ mice (Gautier et al., 2008). PINK1$^{-/-}$ MEFs clearly showed a phenotype of mitochondrial dysfunctions, which is consistent with PD pathogenesis. This phenotype was apparent in a cell growth experiment using medium containing galactose instead of glucose (Fig. 1B). Mitochondrial fragmentation was observed when PINK1$^{-/-}$ MEFs grew in the galactose medium (Fig. 1C), which was consistent with previous reports (Exner et al., 2007; Grünewald et al., 2009). Our results have unveiled that the PINK1$^{-/-}$ MEF line could be a potential PD model, presenting growth retardation due to decreased mitochondrial respiration activity. Thus, the PINK1$^{-/-}$ MEFs are a useful tool for evaluating the role of PINK1 in mitochondrial dysfunction and relevant to PD.

In PINK1$^{-/-}$ MEFs, mitochondrial membrane potential was decreased compared with that in littermate wild-type MEFs (Figs. 2C and D), as reported previously for PINK1 knock-down HeLa cells (Exner et al., 2007) and stable PINK1 knock-down neuroblastoma cell lines (Sandebring et al., 2009). This is a key event during elimination of mitochondria. Mitochondrial fission followed by selective fusion segregates damaged mitochondria, which decreases their membrane potential, and permits their removal by autophagy (Twig et al., 2008). The PINK1–parkin pathway is thought to have a crucial role in this mitochondrial elimination mechanism (Geisler et al., 2010; Kawajiri et al., 2010; Matsuda et al., 2010; Narendra et al., 2008, 2010; Vives-Bauza et al., 2010). To clarify what caused the decrease in mitochondrial membrane potential, we performed a modular kinetic analysis using isolated mitochondria (Fig. 3). This analyzes the kinetics of the whole of oxidative phosphorylation divided into three modules connected by their common substrate or product, mitochondrial membrane potential ($\Delta\psi$). The modules are include one $\Delta\psi$-producer (substrate oxidation) and two $\Delta\psi$-consumers (phosphorylating system and proton leak) (Brand, 1990). To decrease $\Delta\psi$, the $\Delta\psi$-producer should be down-regulated and/or $\Delta\psi$-consumers should be up-regulated. As cellular ATP levels were decreased compared with those in littermate wild-type MEFs (Fig. 2B), it is unlikely that the phosphorylating system is up-regulated. Indeed, the kinetics of the phosphorylation module were not altered (Fig. 3C). The other $\Delta\psi$-consumer, proton leak,

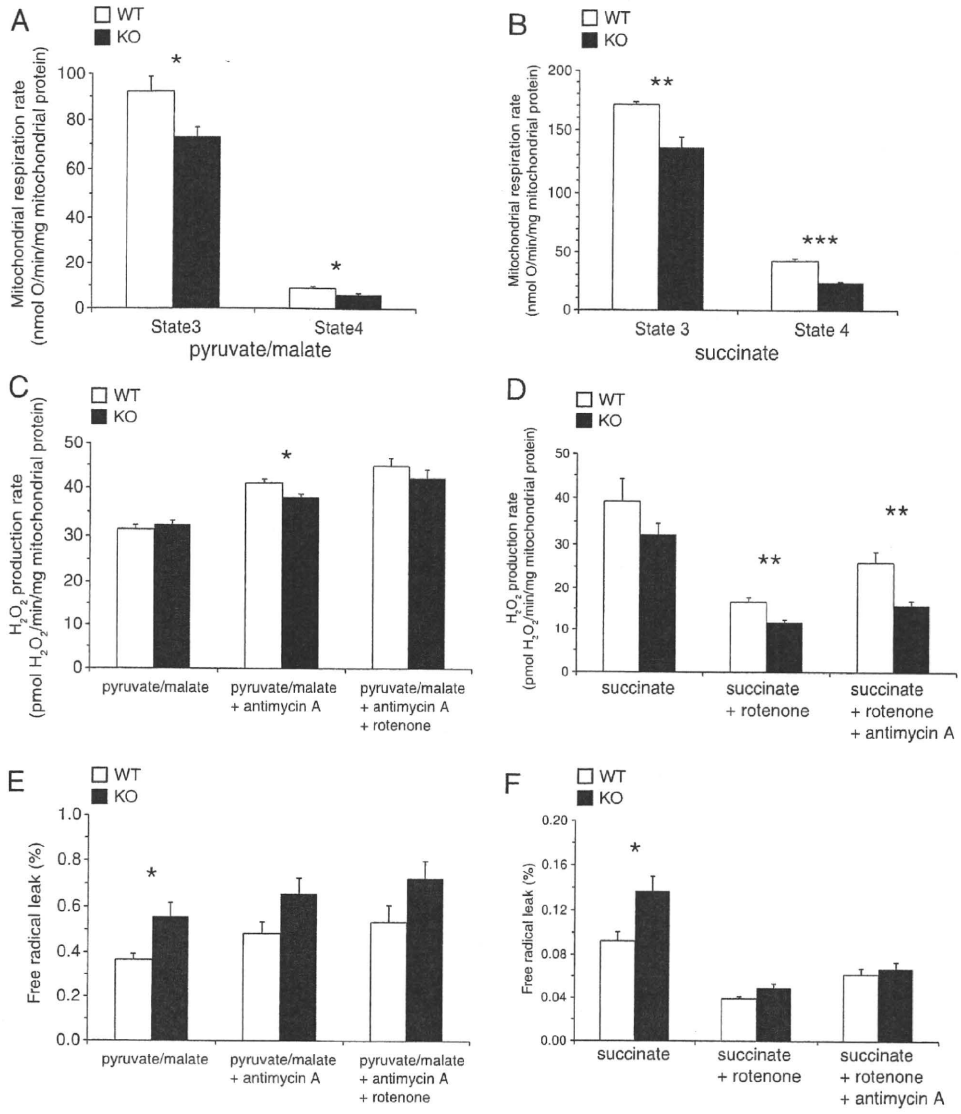

Fig. 4. Oxygen consumption rate and H_2O_2 production rate of mitochondria isolated from PINK1$^{+/+}$ and $^{-/-}$ MEFs. Open bars, PINK1$^{+/+}$ MEFs; closed bars, PINK1$^{-/-}$ MEFs. (A) State 3 and State 4 respiration rate of mitochondria with pyruvate/malate as a respiratory substrate. (B) State 3 and State 4 respiration rate of mitochondria with succinate as a respiratory substrate. Data were derived from the results of modular kinetic analysis (Fig. 3). State 3 respiration rates were the kinetic start points of the $\Delta\psi$-consumers (the sum of the phosphorylating system and proton leak). State 4 respiration rates were average values of the respiration rates at the kinetic start points of substrate oxidation and proton leak. (C, D) Mitochondrial H_2O_2 production rate with pyruvate/malate (C) or succinate (D) as a respiratory substrate. (E, F) Percentage free radical leak (FRL) for State 4 respiration with pyruvate/malate (E) or succinate (F) as a respiratory substrate. Error bars indicate SEM ($n = 5$ and 4 independent mitochondrial preparations for pyruvate/malate and succinate respiration, respectively). $^*P<0.05$; $^{**}P<0.01$; $^{***}P<0.001$.

which partially dissipates the membrane potential without ATP synthesis, was also not changed (Fig. 3B). Therefore, the decrease in membrane potential caused by loss of PINK1 is likely to have been caused only by lower activity of the $\Delta\psi$-producer, substrate oxidation (Fig. 3A). This is the first report showing that mitochondrial membrane potential decrease caused by loss of PINK1, which is the key event for the following mitochondrial elimination, was not due to proton leak, but to respiratory chain defects. We used only succinate (a complex II-linked substrate) as a respiratory substrate in the modular kinetic analysis for technical reasons. However, complex I-linked respiration (pyruvate/malate) was also decreased in PINK1$^{-/-}$ MEFs like succinate respiration (Fig. 4A).

The mitochondrial respiration rates in State 4 were decreased in PINK1$^{-/-}$ MEFs, and consequently, the proportions of free radical leak were significantly higher in PINK1$^{-/-}$ MEFs than in PINK1$^{+/+}$ MEFs (Figs. 4E and F). Because the differences disappeared with addition of rotenone (complex I inhibitor, which inhibits reverse electron flow from coenzyme Q to complex I), ROS generation enhanced by loss of PINK1 was mostly from complex I. These results are partially consistent with those in previous reports, suggesting that MPTP and rotenone induce neuronal cell death by inhibiting complex I activity, leading to a PD-like phenotype (Dauer and Przedborski, 2003; Jackson-Lewis and Przedborski, 2007; Trojanowski, 2003).

In this study, we developed an *in vitro* PD model, the PINK1$^{-/-}$ MEF line, and established the experimental conditions for cell growth to detect mitochondrial dysfunction. This is the first report showing that complete ablation of PINK1 causes a decrease in mitochondrial membrane potential, which is not due to proton leak, but to respiratory chain defects.

Supplementary materials related to this article can be found online at doi:10.1016/j.nbd.2010.08.027.

Acknowledgments

This work was supported by a Grant-in-Aid for Scientific Research for Young Scientists (B) from JSPS (T.A. and S.Saiki), a JSPS fellowship (T.A.), Nagao Memorial Fund (S. Saiki) and a Grant from Takeda Scientific Foundation (S. Saiki and T.A.). We thank Dr. Noriyuki Matsuda for assistance to obtain immortalized cells.

References

Abou-Sleiman, P.M., Muqit, M.M., Wood, N.W., 2006. Expanding insights of mitochondrial dysfunction in Parkinson's disease. Nat. Rev. Neurosci. 7, 207–219.

Amo, T., Brand, M.D., 2007. Were inefficient mitochondrial haplogroups selected during migrations of modern humans? A test using modular kinetic analysis of coupling in mitochondria from cybrid cell lines. Biochem. J. 404, 345–351.

Barja, G., Cadenas, S., Rojas, C., Pérez-Campo, R., López-Torres, M., 1994. Low mitochondrial free radical production per unit O_2 consumption can explain the simultaneous presence of high longevity and high aerobic metabolic rate in birds. Free Radic. Res. 21, 317–327.

Brand, M.D., 1990. The proton leak across the mitochondrial inner membrane. Biochim. Biophys. Acta 1018, 128–133.

Brand, M.D., 1995. Measurement of mitochondrial protonmotive force. In: Brown, G.C., Cooper, C.E. (Eds.), Bioenergetics, a practical approach. IRL Press, Oxford, pp. 39–62.

Brand, M.D., 1998. Top-down elasticity analysis and its application to energy metabolism in isolated mitochondria and intact cells. Mol. Cell. Biochem. 184, 13–20.

Brand, M.D., Chien, L.F., Diolez, P., 1994. Experimental discrimination between proton leak and redox slip during mitochondrial electron transport. Biochem. J. 297, 27–29.

Chu, C.T., 2010. Tickled PINK1: mitochondrial homeostasis and autophagy in recessive Parkinsonism. Biochim. Biophys. Acta 1802, 20–28.

Clark, I.E., Dodson, M.W., Jiang, C., Cao, J.H., Huh, J.R., Seol, J.H., Yoo, S.J., Hay, B.A., Guo, M., 2006. *Drosophila pink1* is required for mitochondrial function and interacts genetically with *parkin*. Nature 441, 1162–1166.

Dauer, W., Przedborski, S., 2003. Parkinson's disease: mechanisms and models. Neuron 39, 889–909.

Exner, N., Treske, B., Paquet, D., Holmstrom, K., Schiesling, C., Gispert, S., Carballo-Carbajal, I., Berg, D., Hoepken, H.H., Gasser, T., Krüger, R., Winklhofer, K.F., Vogel, F., Reichert, A.S., Auburger, G., Kahle, P.J., Schmid, B., Haass, C., 2007. Loss-of-function of human PINK1 results in mitochondrial pathology and can be rescued by parkin. J. Neurosci. 27, 12413–12418.

Gandhi, S., Wood-Kaczmar, A., Yao, Z., Plun-Favreau, H., Deas, E., Klupsch, K., Downward, J., Latchman, D.S., Tabrizi, S.J., Wood, N.W., Duchen, M.R., Abramov, A.Y., 2009. PINK1-associated Parkinson's disease is caused by neuronal vulnerability to calcium-induced cell death. Mol. Cell 33, 627–638.

Gautier, C.A., Kitada, T., Shen, J., 2008. Loss of PINK1 causes mitochondrial functional defects and increased sensitivity to oxidative stress. Proc. Natl. Acad. Sci. U. S. A. 105, 11364–11369.

Geisler, S., Holmström, K.M., Skujat, D., Fiesel, F.C., Rothfuss, O.C., Kahle, P.J., Springer, W., 2010. PINK1/Parkin-mediated mitophagy is dependent on VDAC1 and p62/SQSTM1. Nat. Cell Biol. 12, 119–131.

Gispert, S., Ricciardi, F., Kurz, A., Azizov, M., Hoepken, H.H., Becker, D., Voos, W., Leuner, K., Müller, W.E., Kudin, A.P., Kunz, W.S., Zimmermann, A., Roeper, J., Wenzel, D., Jendrach, M., García-Arencíbia, M., Fernández-Ruiz, J., Huber, L., Rohrer, H., Barrera, M., Reichert, A.S., Rüb, U., Chen, A., Nussbaum, R.L., Auburger, G., 2009. Parkinson phenotype in aged PINK1-deficient mice is accompanied by progressive mitochondrial dysfunction in absence of neurodegeneration. PLoS One 4, e5777.

Grünewald, A., Gegg, M.E., Taanman, J.W., King, R.H., Kock, N., Klein, C., Schapira, A.H., 2009. Differential effects of PINK1 nonsense and missense mutations on mitochondrial function and morphology. Exp. Neurol. 219, 266–273.

Haque, M.E., Thomas, K.J., D'Souza, C., Callaghan, S., Kitada, T., Slack, R.S., Fraser, P., Cookson, M.R., Tandon, A., Park, D.S., 2008. Cytoplasmic Pink1 activity protects neurons from dopaminergic neurotoxin MPTP. Proc. Natl. Acad. Sci. U. S. A. 105, 1716–1721.

Hofhaus, G., Johns, D.R., Hurko, O., Attardi, G., Chomyn, A., 1996. Respiration and growth defects in transmitochondrial cell lines carrying the 11778 mutation associated with Leber's hereditary optic neuropathy. J. Biol. Chem. 271, 13155–13161.

Jackson-Lewis, V., Przedborski, S., 2007. Protocol for the MPTP mouse model of Parkinson's disease. Nat. Protoc. 2, 141–151.

Kawajiri, S., Saiki, S., Sato, S., Sato, F., Hatano, T., Eguchi, H., Hattori, N., 2010. PINK1 is recruited to mitochondria with parkin and associates with LC3 in mitophagy. FEBS Lett. 584, 1073–1079.

Kim, Y., Park, J., Kim, S., Song, S., Kwon, S.K., Lee, S.H., Kitada, T., Kim, J.M., Chung, J., 2008. PINK1 controls mitochondrial localization of Parkin through direct phosphorylation. Biochem. Biophys. Res. Commun. 377, 975–980.

King, M.P., Attardi, G., 1989. Human cells lacking mtDNA: repopulation with exogenous mitochondria by complementation. Science 246, 500–503.

Lambert, A.J., Buckingham, J.A., Boysen, H.M., Brand, M.D., 2010. Low complex I content explains the low hydrogen peroxide production rate of heart mitochondria from the long-lived pigeon, Columba livia. Aging Cell 9, 78–91.

Liu, W., Vives-Bauza, C., Acin-Perez, R., Yamamoto, A., Tan, Y., Li, Y., Magrane, J., Stavarache, M.A., Shaffer, S., Chang, S., Kaplitt, M.G., Huang, X.Y., Beal, M.F., Manfredi, G., Li, C., 2009. PINK1 defect causes mitochondrial dysfunction, proteasomal deficit and alpha-synuclein aggregation in cell culture models of Parkinson's disease. PLoS One 4, e4597.

Matsuda, N., Sato, S., Shiba, K., Okatsu, K., Saisho, K., Gautier, C.A., Sou, Y.S., Saiki, S., Kawajiri, S., Sato, F., Kimura, M., Komatsu, M., Hattori, N., Tanaka, K., 2010. PINK1 stabilized by mitochondrial depolarization recruits Parkin to damaged mitochondria and activates latent Parkin for mitophagy. J. Cell Biol. 189, 211–221.

Narendra, D., Tanaka, A., Suen, D.F., Youle, R.J., 2008. Parkin is recruited selectively to impaired mitochondria and promotes their autophagy. J. Cell Biol. 183, 795–803.

Narendra, D.P., Jin, S.M., Tanaka, A., Suen, D.F., Gautier, C.A., Shen, J., Cookson, M.R., Youle, R.J., 2010. PINK1 is selectively stabilized on impaired mitochondria to activate Parkin. PLoS Biol. 8, e1000298.

Park, J., Lee, S.B., Lee, S., Kim, Y., Song, S., Kim, S., Bae, E., Kim, J., Shong, M., Kim, J.M., Chung, J., 2006. Mitochondrial dysfunction in *Drosophila PINK1* mutants is complemented by *parkin*. Nature 441, 1157–1161.

Pridgeon, J.W., Olzmann, J.A., Chin, L.S., Li, L., 2007. PINK1 protects against oxidative stress by phosphorylating mitochondrial chaperone TRAP1. PLoS Biol. 5, e172.

Reitzer, L.J., Wice, B.M., Kennell, D., 1979. Evidence that glutamine, not sugar, is the major energy source for cultured HeLa cells. J. Biol. Chem. 254, 2669–2676.

Reynafarje, B., Costa, L.E., Lehninger, A.L., 1985. O_2 solubility in aqueous media determined by a kinetic method. Anal. Biochem. 145, 406–418.

Sandebring, A., Thomas, K.J., Beilina, A., van der Brug, M., Cleland, M.M., Ahmad, R., Miller, D.W., Zambrano, I., Cowburn, R.F., Behbahani, H., Cedazo-Mínguez, A., Cookson, M.R., 2009. Mitochondrial alterations in PINK1 deficient cells are influenced by calcineurin-dependent dephosphorylation of dynamin-related protein 1. PLoS One 4, e5701.

Trojanowski, J.Q., 2003. Rotenone neurotoxicity: a new window on environmental causes of Parkinson's disease and related brain amyloidoses. Exp. Neurol. 179, 6–8.

Twig, G., Elorza, A., Molina, A.J., Mohamed, H., Wikstrom, J.D., Walzer, G., Stiles, L., Haigh, S.E., Katz, S., Las, G., Alroy, J., Wu, M., Py, B.F., Yuan, J., Deeney, J.T., Corkey, B. E., Shirihai, O.S., 2008. Fission and selective fusion govern mitochondrial segregation and elimination by autophagy. EMBO J. 27, 433–446.

Valente, E.M., Abou-Sleiman, P.M., Caputo, V., Muqit, M.M., Harvey, K., Gispert, S., Ali, Z., Del Turco, D., Bentivoglio, A.R., Healy, D.G., Albanese, A., Nussbaum, R., González-Maldonado, R., Deller, T., Salvi, S., Cortelli, P., Gilks, W.P., Latchman, D.S., Harvey, R.J., Dallapiccola, B., Auburger, G., Wood, N.W., 2004. Hereditary early-onset Parkinson's disease caused by mutations in *PINK1*. Science 304, 1158–1160.

Vives-Bauza, C., Zhou, C., Huang, Y., Cui, M., de Vries, R.L., Kim, J., May, J., Tocilescu, M.A., Liu, W., Ko, H.S., Magrane, J., Moore, D.J., Dawson, V.L., Grailhe, R., Dawson, T.M., Li, C., Tieu, K., Przedborski, S., 2010. PINK1-dependent recruitment of Parkin to mitochondria in mitophagy. Proc. Natl. Acad. Sci. U. S. A. 107, 378–383.

Wood-Kaczmar, A., Gandhi, S., Yao, Z., Abramov, A.Y., Miljan, E.A., Keen, G., Stanyer, L., Hargreaves, I., Klupsch, K., Deas, E., Downward, J., Mansfield, L., Jat, P., Taylor, J., Heales, S., Duchen, M.R., Latchman, D., Tabrizi, S.J., Wood, N.W., 2008. PINK1 is necessary for long term survival and mitochondrial function in human dopaminergic neurons. PLoS One 3, e2455.

Yang, Y., Ouyang, Y., Yang, L., Beal, M.F., McQuibban, A., Vogel, H., Lu, B., 2008. Pink1 regulates mitochondrial dynamics through interaction with the fission/fusion machinery. Proc. Natl. Acad. Sci. U. S. A. 105, 7070–7075.

Published April 19, 2010

PINK1 stabilized by mitochondrial depolarization recruits Parkin to damaged mitochondria and activates latent Parkin for mitophagy

Noriyuki Matsuda,[1] Shigeto Sato,[2] Kahori Shiba,[3] Kei Okatsu,[1] Keiko Saisho,[1] Clement A. Gautier,[4] Yu-shin Sou,[1] Shinji Saiki,[2] Sumihiro Kawajiri,[2] Fumiaki Sato,[3] Mayumi Kimura,[1] Masaaki Komatsu,[1,5] Nobutaka Hattori,[2] and Keiji Tanaka[1]

[1]Laboratory of Frontier Science, Tokyo Metropolitan Institute of Medical Science, Setagaya-ku, Tokyo 156-8506, Japan
[2]Department of Neurology and [3]Research Institute for Diseases of Old Age, Juntendo University School of Medicine, Bunkyo-ku, Tokyo 113-8421, Japan
[4]Center for Neurologic Diseases, Brigham and Women's Hospital, Harvard Medical School, Boston, MA 02115
[5]Precursory Research for Embryonic Science and Technology, Japan Science and Technology Agency, Kawaguchi 332-0012, Japan

Parkinson's disease (PD) is a prevalent neurodegenerative disorder. Recent identification of genes linked to familial forms of PD such as *Parkin* and *PINK1* (*PTEN-induced putative kinase 1*) has revealed that ubiquitylation and mitochondrial integrity are key factors in disease pathogenesis. However, the exact mechanism underlying the functional interplay between Parkin-catalyzed ubiquitylation and PINK1-regulated mitochondrial quality control remains an enigma. In this study, we show that PINK1 is rapidly and constitutively degraded under steady-state conditions in a mitochondrial membrane potential–dependent manner and that a loss in mitochondrial membrane potential stabilizes PINK1 mitochondrial accumulation. Furthermore, PINK1 recruits Parkin from the cytoplasm to mitochondria with low membrane potential to initiate the autophagic degradation of damaged mitochondria. Interestingly, the ubiquitin ligase activity of Parkin is repressed in the cytoplasm under steady-state conditions; however, PINK1-dependent mitochondrial localization liberates the latent enzymatic activity of Parkin. Some pathogenic mutations of PINK1 and Parkin interfere with the aforementioned events, suggesting an etiological importance. These results provide crucial insight into the pathogenic mechanisms of PD.

Introduction

Parkinson's disease (PD) is a very common movement disorder characterized by dopaminergic neuronal loss. The majority of PD cases are sporadic; however, the discovery of genes linked to rare familial forms of this disease has provided important insight into the molecular mechanisms of disease pathogenesis (Moore et al., 2005; Hardy et al., 2006). In 2000, we and others found that dysfunction of an E3 ubiquitin ligase (Imai et al., 2000; Shimura et al., 2000; Zhang et al., 2000) termed Parkin causes autosomal recessive juvenile Parkinsonism (Kitada et al., 1998). Since then, a multitude of papers have been published, but the mechanism by which dysfunction of Parkin causes autosomal recessive juvenile Parkinsonism has largely remained obscure, and claims of pathogenicity remain controversial (Lim, 2007; Matsuda and Tanaka, 2010). In addition, *PINK1* (*PTEN-induced putative kinase 1*) was identified in 2004 as the gene responsible for another form of early-onset PD (Valente et al., 2004). PINK1 functions in mitochondrial maintenance, suggesting that mitochondrial integrity is another key factor in disease pathogenesis (Dodson and Guo, 2007; Schapira, 2008). Intriguingly, genetic studies using *Drosophila melanogaster* revealed that PINK1 and Parkin function in the same pathway, with PINK1 functioning upstream of Parkin (Clark et al., 2006; Park et al., 2006; Yang et al., 2006). Little is known about how PINK1

Correspondence to Noriyuki Matsuda: matsuda-nr@igakuken.or.jp; or Keiji Tanaka: tanaka-kj@igakuken.or.jp

Abbreviations used in this paper: CCCP, carbonyl cyanide m-chlorophenylhydrazone; MEF, mouse embryonic fibroblast; Mt-GFP, mitochondria-targeting GFP; PD, Parkinson's disease.

© 2010 Matsuda et al. This article is distributed under the terms of an Attribution–Noncommercial–Share Alike–No Mirror Sites license for the first six months after the publication date (see http://www.rupress.org/terms). After six months it is available under a Creative Commons License (Attribution–Noncommercial–Share Alike 3.0 Unported license, as described at http://creativecommons.org/licenses/by-nc-sa/3.0/).

Supplemental Material can be found at:
http://jcb.rupress.org/content/suppl/2010/04/18/jcb.200910140.DC1.html

The Rockefeller University Press $30.00
J. Cell Biol. Vol. 189 No. 2 211–221
www.jcb.org/cgi/doi/10.1083/jcb.200910140

THE JOURNAL OF CELL BIOLOGY

Downloaded from jcb.rupress.org on May 26, 2011

Published April 19, 2010

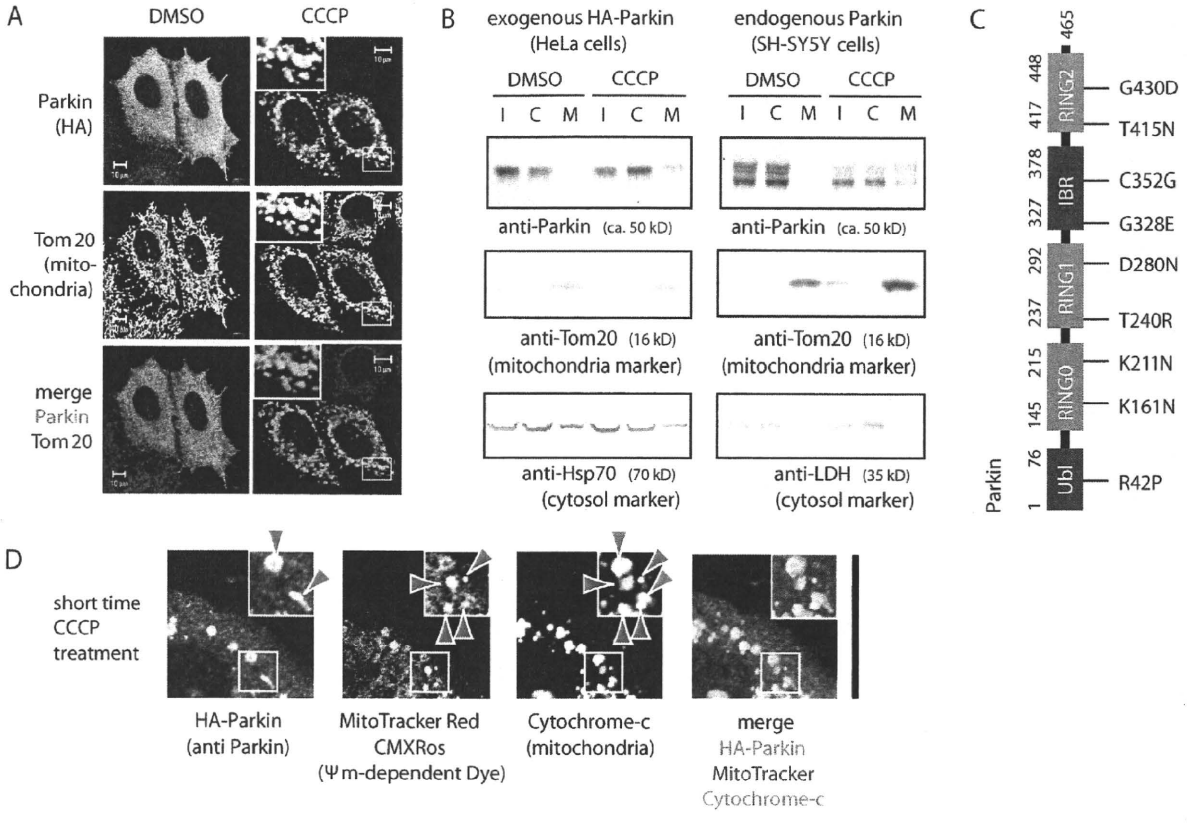

Downloaded from jcb.rupress.org on May 26, 2011

Published April 19, 2010

regulates Parkin, and our knowledge, especially in mammals, of their relationship is limited. In this study, we describe the mechanism underlying the functional interplay between ubiquitylation catalyzed by Parkin and mitochondrial quality control regulated by PINK1.

Results and discussion

Parkin localizes to and ubiquitylates mitochondria with low membrane potential

We initially sought to study the subcellular localization and E3 activity of Parkin using HeLa cells, which reportedly lack a functional *Parkin* gene (Denison et al., 2003). In support of that study, we found that endogenous Parkin was barely detectable in HeLa cells even when PRK8, the best-characterized specific anti-Parkin antibody (Pawlyk et al., 2003), was used (Fig. S1 A). Consequently, HA-Parkin was exogenously introduced into HeLa cells. Under steady-state conditions, HA-Parkin was diffusely localized throughout the cytosol and did not overlap with mitochondria, whereas Parkin was rapidly recruited to the mitochondria when HeLa cells were treated with the mitochondrial uncoupler CCCP (carbonyl cyanide m-chlorophenylhydrazone; Fig. 1 A), as reported by Narendra et al. (2008). Next we tried to confirm the redistribution of Parkin from the cytoplasm to the mitochondria using a biochemical approach. In fractionation experiments, detection of Parkin in the mitochondria-rich fraction was faint, probably because Parkin was weakly associated with the mitochondria and thus unstable during fractionation. Inclusion of the cross-linker DSP (dithiobis[succinimidyl propionate]) significantly strengthened the signal and further confirmed redistribution of exogenous (Fig. 1 B, left) and endogenous (Fig. 1 B, right) Parkin from the cytoplasm to a mitochondria-enriched fraction. (Note that endogenous Parkin in SH-SY5Y cells is detectable as a doublet, which is consistent with a previous study [Pawlyk et al., 2003].) To more convincingly demonstrate that Parkin is selectively recruited to depolarized mitochondria, we used MitoTracker red CMXRos, which accumulates in mitochondria with an intact membrane potential. Incomplete treatment with CCCP can generate cells in which healthy and damaged mitochondria coexist. Under these conditions, signals of Parkin and MitoTracker were mutually exclusive, and Parkin selectively localized on mitochondria with lower MitoTracker red staining (Fig. 1 D), indicating that Parkin was selectively targeted to mitochondria whose membrane potential had been lost.

Subsequently, we performed immunofluorescence staining using an antiubiquitin antibody. Under normal conditions, the ubiquitin signal was spread throughout the cell. In contrast, when cells were treated with CCCP, the ubiquitin signal was concentrated in the mitochondria (Fig. 2, A and B). Mitochondrial ubiquitylation was only observed in Parkin-expressing cells (Fig. 2 A and Fig. S1 B) and disappeared when Parkin mutants deficient in E3 activity (T415N and G430D) were introduced (Fig. 2 A). Triple staining using mitochondria-targeting GFP (Mt-GFP), anti-Parkin, and anti-ubiquitin antibodies further confirmed the colocalization of Parkin, ubiquitin, and mitochondria after CCCP treatment (Fig. 2 C). Staining with single antibodies or Mt-GFP alone indicated that the aforementioned merged data were not derived from channel cross talk (Fig. S1, C and D). These results demonstrate that Parkin ubiquitylates mitochondria in response to a reduction in mitochondrial membrane potential.

Disease-relevant mutations of Parkin impair mitochondrial localization

To confirm that translocation of Parkin to depolarized mitochondria is etiologically important, we selected nine pathogenic mutations and examined their subcellular localization (Fig. 1 C). In vitro experiments have previously shown that two of the mutations (T415N and G430D) in the RING2 domain abolish E3 activity of Parkin, whereas E3 activity is unaffected by the other mutations (Hampe et al., 2006; Matsuda et al., 2006). These mutants were serially introduced into HeLa cells, followed by CCCP treatment, and their subcellular localization was examined. Parkin with the D280N or G328E mutation in RING1 or the IBR (in between RING) domain, respectively, was recruited to the mitochondria in a manner similar to wild-type Parkin (Fig. 1, E and F). In contrast, the other pathogenic mutations altered to some degree the mitochondrial localization of Parkin; in particular, the K161N, K211N, and T240R mutations, which lie in or near the RING0 domain in the linker region (Hristova et al., 2009), severely compromised the mitochondrial localization of Parkin (Fig. 1, E and F). The aforementioned results suggest that mitochondrial localization of Parkin is pathologically significant and that the RING0 domain is important for the translocation of Parkin to the damaged mitochondria.

Parkin exerts E3 activity only when the mitochondrial membrane potential decreases

As shown in Fig. 2 C and Fig. S1 B, mitochondrial ubiquitylation was dependent on Parkin translocation to the mitochondria. Thus, we tried to determine whether the subcellular localization of Parkin modulates its E3 activity. To address this issue, we monitored the E3 activity of Parkin using an

Figure 1. **Mitochondrial localization of Parkin is etiologically important.** (A) HeLa cells expressing HA-Parkin were treated with CCCP or DMSO (control) and then immunostained with the indicated antibodies. (B) HeLa cells stably expressing HA-Parkin or intact SH-SY5Y cells were treated with CCCP or DMSO and subjected to fractionation experiments. I, C, and M indicate input, cytosol-rich supernatant, and mitochondria-rich membrane pellet, respectively. (C) Schematic diagram of disease-relevant mutants of Parkin used in this study. IBR, in between RING; Ubl, ubiquitin like. (D) Polarized mitochondria stained with MitoTracker red (red arrowheads) were not labeled by Parkin. In contrast, damaged mitochondria marked by Parkin (green arrowheads) were not stained with MitoTracker red. (E) HeLa cells expressing HA-Parkin with various pathogenic mutations were treated with CCCP, followed by immunocytochemistry. (A, D, and E) Higher magnification views of the boxed areas are shown in the insets. (F) Parkin colocalization with mitochondria was analyzed in >100 cells per mutation. Example figures indicative of robust colocalization (counted as 1), weak colocalization (counted as 0.5), and no colocalization (counted as 0) are shown. Error bars represent the mean ± SD values of at least three experiments. Bars: (A, E, and F) 10 µm; (D) 30 µm.

Downloaded from jcb.rupress.org on May 26, 2011

Published April 19, 2010

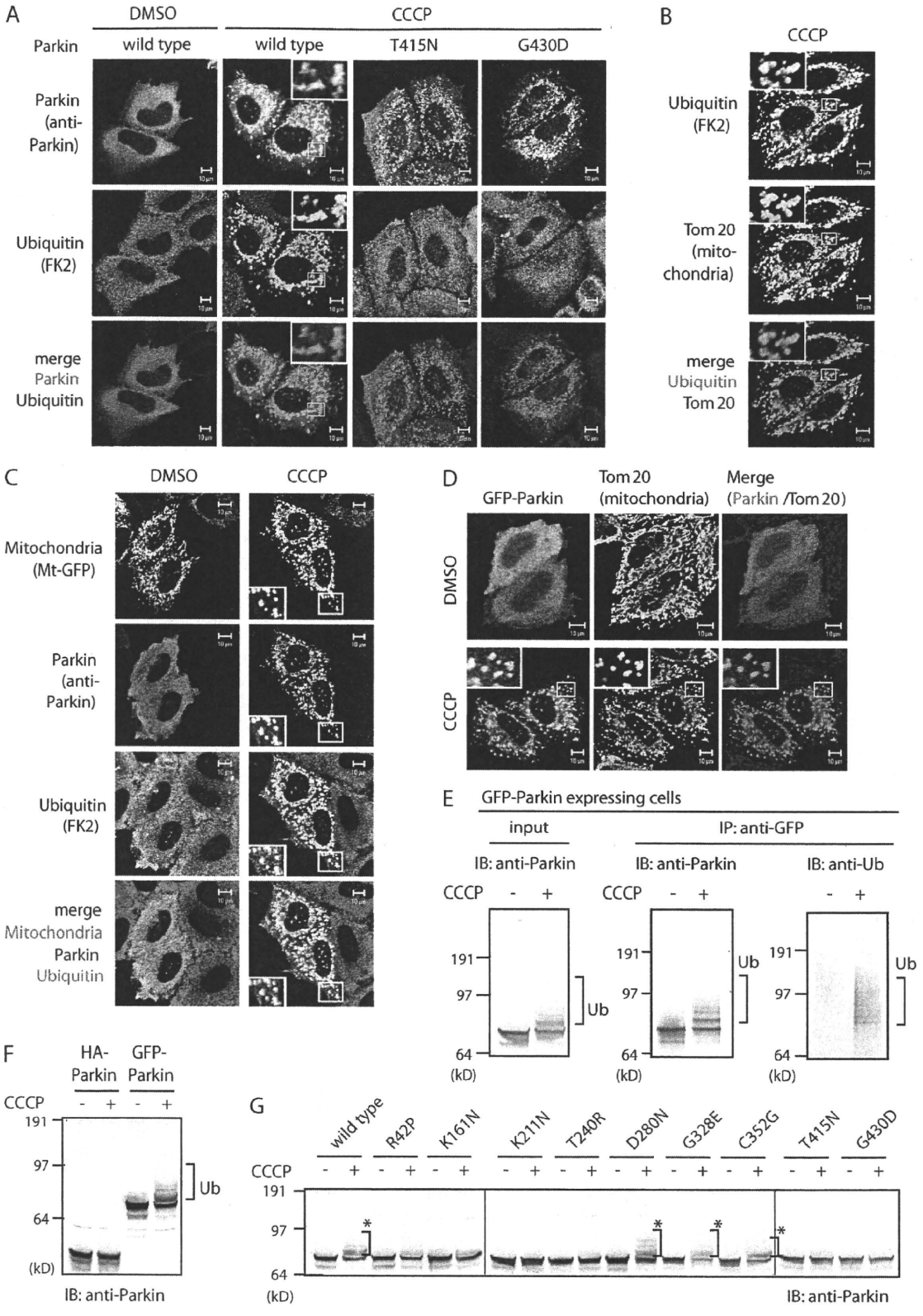

Figure 2. **Parkin exerts E3 activity only when the mitochondrial membrane potential is decreased.** (A) HeLa cells expressing wild-type Parkin or E3-inactivating mutations were treated with CCCP and then immunostained with the indicated antibodies. When E3-inactivating mutations were introduced into Parkin, the mitochondrial ubiquitylation signal disappeared. (B and C) HeLa cells expressing HA-Parkin (B) or expressing both Mt-GFP and HA-Parkin (C)

Downloaded from jcb.rupress.org on May 26, 2011

Published April 19, 2010

artificial substrate fused to Parkin. In vitro experiments have shown that Parkin can ubiquitylate an N-terminally fused lysine-rich protein as a pseudosubstrate (Matsuda et al., 2006). Similar ubiquitylation of pseudosubstrates even in the cytoplasm under normal conditions in vivo would be evidence that the E3 activity is constitutive; otherwise, E3 activity of Parkin is dependent on mitochondrial retrieval. A GFP tag is lysine rich and thus a good candidate for an in vivo pseudosubstrate, whereas an HA tag possesses no lysine residues and thus cannot function as a pseudosubstrate. GFP- and HA-Parkin expressed in HeLa cells treated with CCCP were both recruited to damaged mitochondria (Figs. 1 A and 2 D), but interestingly, a higher molecular mass population of only GFP-Parkin was observed (Fig. 2 F). Immunoprecipitation experiments demonstrated that GFP-Parkin was indeed ubiquitylated (Fig. 2 E). This was not based on autoubiquitylation of Parkin itself because mitochondria-associated HA-Parkin did not undergo ubiquitylation after CCCP treatment (Fig. 2 F and not depicted). Moreover, ubiquitylation of GFP-Parkin was absent in the T415N and G430D mutants, which lack E3 activities, suggesting that ubiquitylation of GFP-Parkin is not derived from other E3s (Fig. 2 G). The K161N and K211N mutants that impaired mitochondrial localization also inhibited ubiquitylation of GFP-Parkin (Fig. 2 G). Collectively, the aforementioned results indicate that Parkin ubiquitylates fused GFP only when it is retrieved to the mitochondria, suggesting that the latent E3 activity of Parkin is dependent on decreased mitochondrial membrane potential.

PINK1 localization is stabilized by damaged mitochondria

Recessive mutations in the human *PINK1* gene are also the cause of autosomal recessive early-onset PD (Valente et al., 2004). We next examined whether the subcellular localization of PINK1 was affected by mitochondrial membrane potential. As reported previously (Valente et al., 2004; Beilina et al., 2005; Takatori et al., 2008), N-terminal Myc– or N-terminal Flag–tagged PINK1 clearly localized to the mitochondria, whereas C-terminal Flag– or C-terminal V5–tagged PINK1 mainly localized to the cytoplasm (Fig. 3 A and not depicted). Exogenous nontagged PINK1 also localized to the cytoplasm under steady-state conditions (Fig. 3 B), suggesting that mitochondrial localization of PINK1 is an artifact of the N-terminal epitope. More importantly, similar to Parkin, untagged PINK1 and C-terminal Flag– or C-terminal V5–tagged PINK1 localized to the mitochondria after CCCP treatment (Fig. 3, A and B; and not depicted). These results suggest that the subcellular localization of PINK1 is also regulated by the mitochondrial membrane potential.

We next sought to determine the subcellular localization of endogenous PINK1. Immunocytochemical experiments showed, as reported previously (Zhou et al., 2008), that the endogenous PINK1 signal was barely detectable in HeLa cells under steady-state conditions. However, a decrease in mitochondrial membrane potential resulted in a mitochondria-associated PINK1 signal (Fig. 3, C and D). We found that CCCP treatment promoted the gradual accumulation of endogenous PINK1 in immunoblots as well (Fig. 3 E) and the presence of endogenous PINK1 in a mitochondria-enriched fraction (Fig. 3 F). More importantly, when CCCP was washed out, the accumulated endogenous PINK1 rapidly disappeared (within 30 min) both in the presence and absence of cycloheximide (Fig. 3 G and not depicted). Moreover, the N-terminal 34 aa of PINK1 sufficiently recruited GFP to the mitochondria even in the absence of CCCP (Fig. 3 H). These results support the hypothesis in which PINK1 is constantly transported to the mitochondria but is rapidly degraded in a membrane potential–dependent manner. We speculate that PINK1 is stabilized by a decrease in mitochondrial membrane potential and, as a result, accumulates in depolarized mitochondria.

PINK1 normally exists as either a long (~60 kD) or a short (~50 kD) protein. Because the canonical mitochondria-targeting signal (matrix-targeting signal) is cleaved after import into the mitochondria, the long form has been designated as the precursor and the short form as the mature PINK1 (Beilina et al., 2005; Silvestri et al., 2005). The short (processed) form of PINK1 was clearly detected when untagged PINK1 was overexpressed (Fig. 3 E, sixth lane); however, this form of endogenous PINK1 was rarely detectable after CCCP treatment (Fig. 3 E, the first through the fifth lanes). Our subcellular localization study of endogenous PINK1 after CCCP treatment showed that the long form was recovered in the mitochondrial fraction (Fig. 3 F), suggesting that it is not the preimport precursor form. Moreover, by monitoring the degradation process of PINK1 after recovery of membrane potential, we realized that the short form of PINK1 transiently appeared soon after CCCP was washed out and then later disappeared (Fig. 3 G), suggesting that the processed form of PINK1 is an intermediate in membrane potential–dependent degradation. In conclusion, these results imply that PINK1 cleavage dose not reflect a canonical maturation process accompanying mitochondrial import as initially thought.

PINK1 retrieves Parkin from the cytoplasm to the mitochondria

Because previous studies revealed that PINK1 functions upstream of Parkin (Clark et al., 2006; Park et al., 2006; Yang et al., 2006; Exner et al., 2007), we next examined the potential role of PINK1 in the mitochondrial recruitment of Parkin. To obtain clear-cut conclusions, we set up our experimental system using mouse embryonic fibroblasts (MEFs) derived from control

were treated with CCCP or DMSO (control) and then immunostained with the indicated antibodies. (D) Localization of GFP-Parkin to the mitochondria after CCCP treatment. (A–D) Higher magnification views of the boxed areas are shown in the insets. (E) HeLa cell lysates expressing GFP-Parkin were immunoprecipitated by anti-GFP antibody, followed by immunoblotting with the indicated antibodies. (F) Straight immunoblotting of HA- and GFP-Parkin in the absence or presence of CCCP. Note the slower migrating ladders derived from ubiquitylation (Ub) in only the GFP-Parkin with CCCP lane. (G) GFP-Parkin–expressing HeLa cells with various pathogenic mutations (Fig. 1 C) were treated with CCCP and subjected to immunoblotting. Asterisks show ubiquitylation of GFP-Parkin. Vertical black lines indicate that intervening lanes have been spliced out. IB, immunoblot; IP, immunoprecipitation. Bars, 10 µm.

Downloaded from jcb.rupress.org on May 26, 2011

Published April 19, 2010

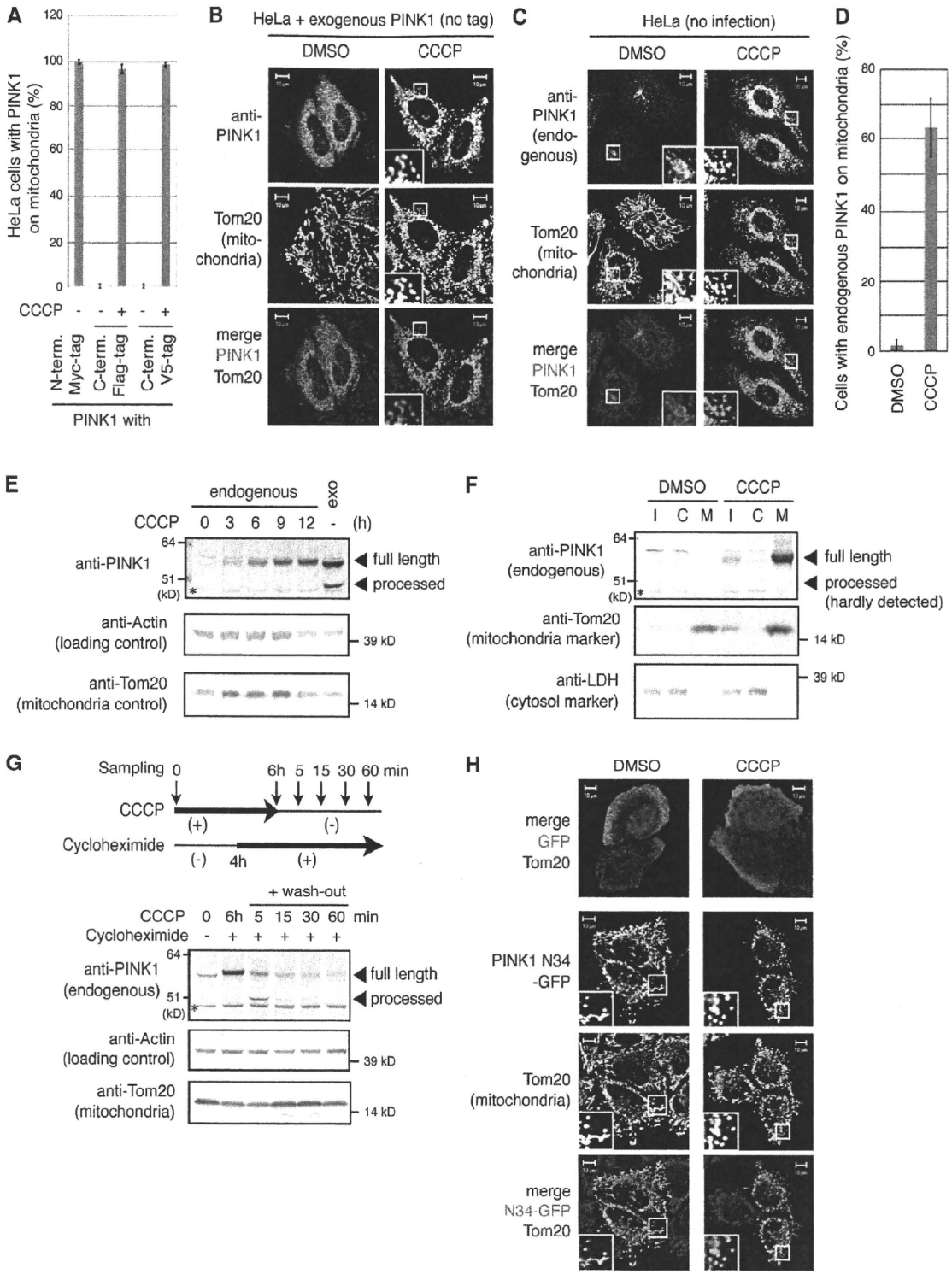

Figure 3. **PINK1 is constitutively degraded in a mitochondrial membrane potential–dependent manner and localizes to depolarized mitochondria.** (A) The number of HeLa cells with N-terminal– or C-terminal–tagged PINK1 localized to the mitochondria was counted in >100 cells. (B and C) Exogenous non-tagged PINK1 (B) or endogenous PINK1 (C) in HeLa cells was immunostained with the indicated antibodies. (D) The number of HeLa cells with endogenous PINK1 localized to the mitochondria was counted as in A. (A and D) Error bars represent the mean ± SD values of least three experiments. (E) Endogenous PINK1 gradually accumulated after CCCP treatment. The first through the fifth lanes show endogenous PINK1, and the sixth lane shows overexpressed untagged PINK1. Note that the asterisk indicates a cross-reacting band because it was not affected by overproduction of untagged PINK1. (F) Subcellular fractionation of endogenous PINK1. Intact SH-SY5Y cells were treated with CCCP or DMSO and subjected to fractionation experiments (same sample as

Downloaded from jcb.rupress.org on May 26, 2011

Published April 19, 2010

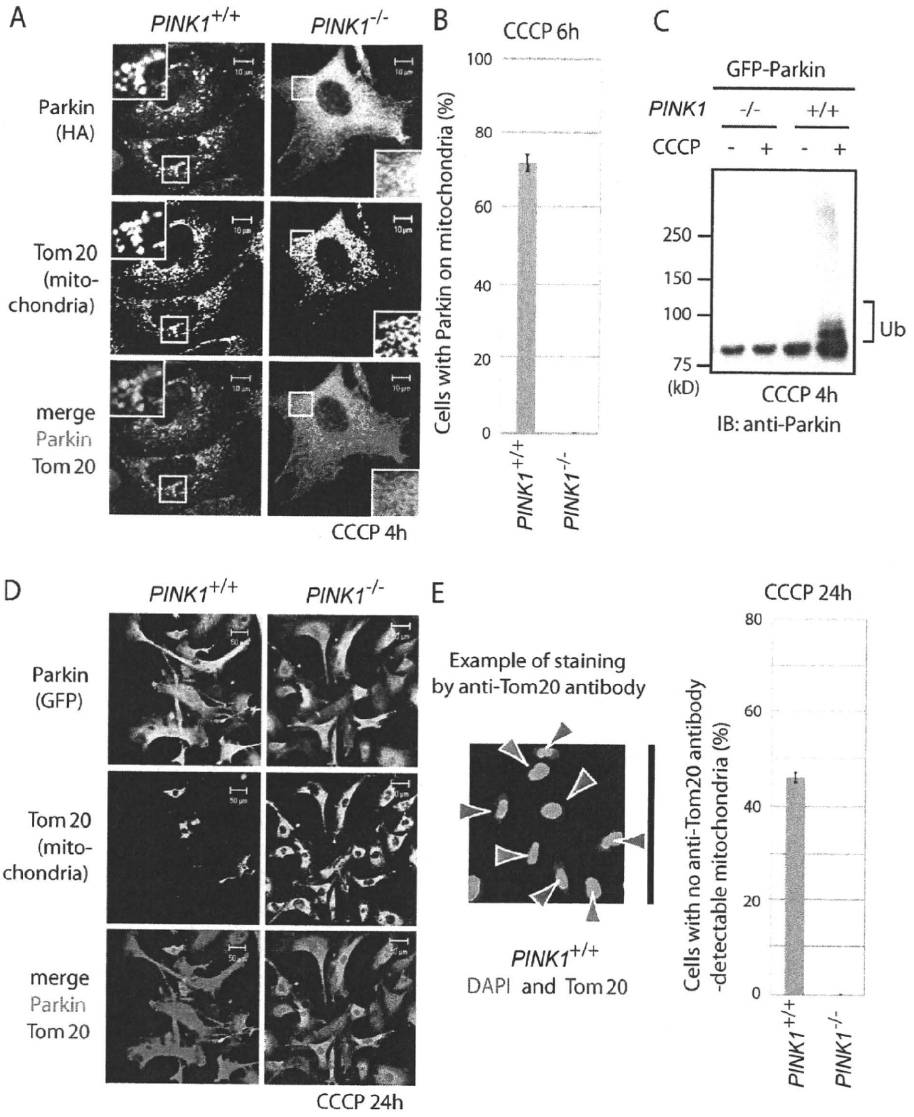

Figure 4. **PINK1 recruits cytoplasmic Parkin to damaged mitochondria.** (A) *PINK1* knockout (*PINK1* $^{-/-}$) or control (*PINK1*$^{+/+}$) MEFs were transfected with HA-Parkin, treated with CCCP, and subjected to immunocytochemistry with the indicated antibodies. Higher magnification views of the boxed areas are shown in the insets. (B) The number of MEFs with Parkin localized to the mitochondria was counted as in Fig. 3 A. (C and D) Neither activation of Parkin nor mitochondrial degradation was observed in *PINK1* $^{-/-}$ MEFs. MEFs stably expressing GFP-Parkin were treated with CCCP for 4 h and subjected to immunoblotting (C) or for 24 h, followed by immunocytochemistry (D). IB, immunoblot; Ub, ubiquitylation. (E) The number of MEFs without anti-Tom20 antibody–detectable mitochondria was counted as in Fig. 3 A. In the example figure (left), blue arrowheads indicate cells without anti-Tom20 antibody–detectable mitochondria, and red arrowheads indicate cells harboring anti-Tom20 antibody–detectable mitochondria. (B and E) Error bars represent the mean ± SD values of least three experiments. Bars: (A) 10 µm; (D) 50 µm; (E) 150 µm.

(*PINK1*$^{+/+}$) or *PINK1* knockout (*PINK1* $^{-/-}$) mouse (Gautier et al., 2008). Endogenous Parkin is undetectable in MEFs (Fig. S1 A); consequently, HA- or GFP-Parkin was introduced into these cells by retroviral transfection (Kitamura et al., 2003). In control MEFs (*PINK1*$^{+/+}$), Parkin was selectively recruited to the mitochondria after CCCP treatment (Fig. 4 A) and subsequently resulted in the disappearance of the mitochondria (Fig. 4, D and E). This mitochondrial clearance was considerably impeded by *Atg7* (essential gene for autophagy) knockout (Fig. S2; Komatsu et al., 2005), suggesting that Parkin degrades mitochondria by selective autophagy as reported previously (Narendra et al., 2008). In sharp contrast, Parkin was not

Fig. 1 B). I, C, and M indicate input, cytosol-rich supernatant, and the mitochondria-rich membrane pellet, respectively. (G) HeLa cells were treated with CCCP and cycloheximide as depicted, followed by immunoblotting with the indicated antibodies. LDH, lactate dehydrogenase. (F and G) Asterisks indicate a cross-reacting band. (H) N-terminal 34 aa of PINK1 recruited GFP to the mitochondria both in the absence and presence of CCCP. The top panel shows control HeLa cells expressing only GFP. (B, C, and H) Higher magnification views of the boxed areas are shown in the insets. Bars, 10 µm.

Downloaded from jcb.rupress.org on May 26, 2011

Published April 19, 2010

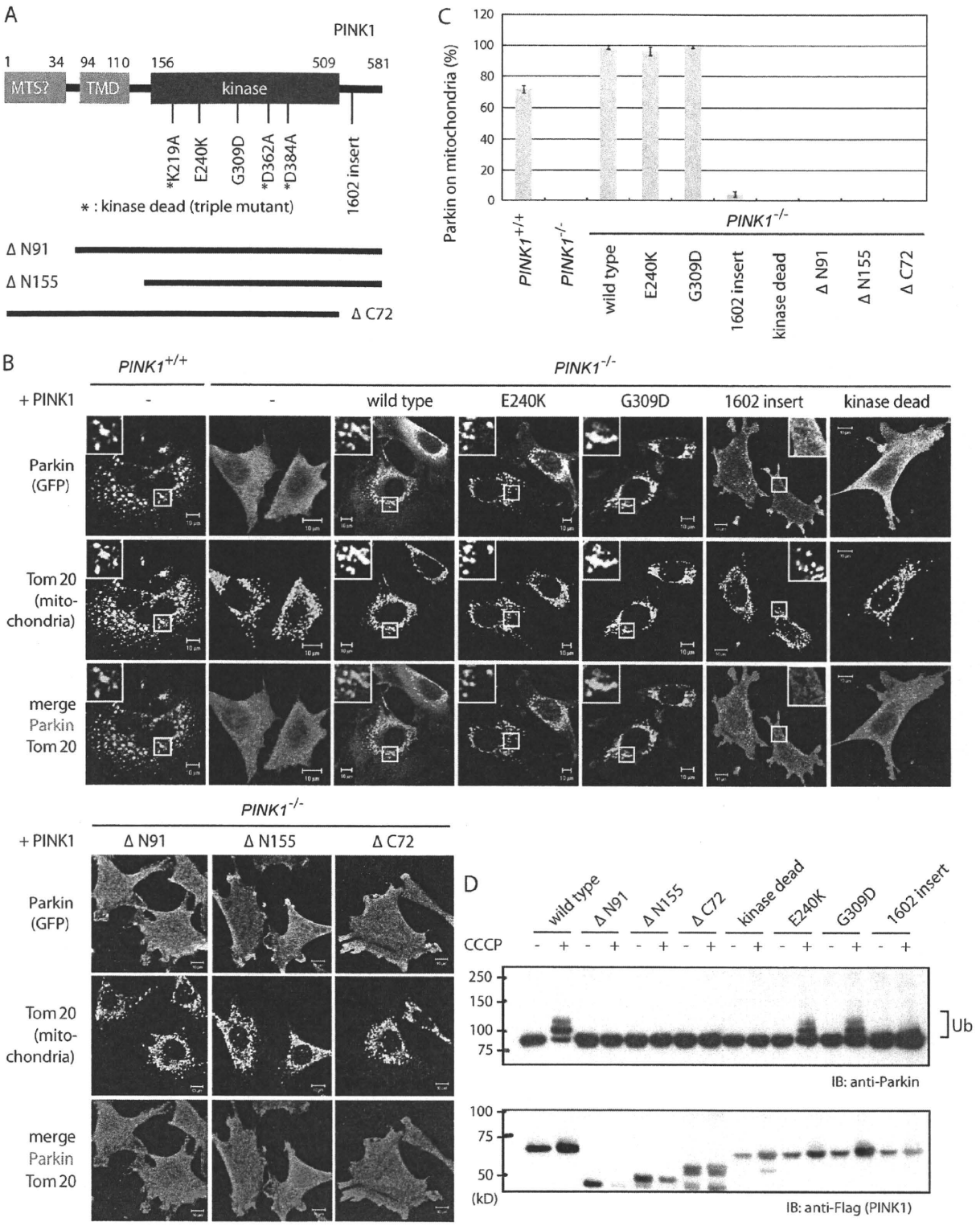

Figure 5. **Kinase activity and mitochondrial targeting of PINK1 is imperative for mitochondrial localization of Parkin.** (A) Schematic depiction of pathogenic and deletion mutants of PINK1 used in this study. MTS, mitochondria-targeting sequence; TMD, transmembrane domain. (B) Subcellular localization of Parkin in *PINK1* $^{-/-}$ cells complemented by various pathogenic and deletion mutants of PINK1-Flag. Cells were treated with CCCP. Higher magnification views of the boxed areas are shown in the insets. (C) The number of cells with Parkin-positive mitochondria was counted as in Fig. 3 A. Error bars represent the mean ± SD values of least three experiments. (D) *PINK1* $^{-/-}$ MEFs complemented by various PINK1 mutants were treated with CCCP and subjected to immunoblotting using anti-Parkin or anti-Flag (tag of PINK1) antibodies. IB, immunoblot; Ub, ubiquitylation. Bars, 10 μm.

Downloaded from jcb.rupress.org on May 26, 2011

Published April 19, 2010

translocated to the mitochondria in *PINK1* knockout (*PINK1*$^{-/-}$) MEFs after CCCP treatment (Fig. 4, A and B). Subsequent activation of Parkin and mitochondrial degradation were also completely impeded (Fig. 4, C–E). To exclude the possible role of retroviral integration of Parkin in the aforementioned phenotype, we checked whether reintroduction of PINK1 rescued this phenotype. Untagged or C-terminal Flag–tagged PINK1 complemented the mislocalization of Parkin in *PINK1*$^{-/-}$ MEFs (Fig. 5, B and C; and not depicted), confirming that the aforementioned defects were caused by the loss of PINK1.

To examine whether pathogenic mutations of PINK1 affect its mitochondrial localization, we expressed PINK1 mutants harboring the missense mutations E240K and G309D, or a CAA nucleotide insertion behind C1602 (referred to hereafter as 1602-insert) in *PINK1*$^{-/-}$ MEFs. Similar to wild-type PINK1, these PINK1 mutants colocalized with mitochondria after CCCP treatment (Fig. S3). Next, GFP-Parkin was introduced into these cells to examine whether pathogenic mutations of PINK1 affect the mitochondrial localization and activation of Parkin. The E240K and G309D mutants restored the mitochondrial localization and activation of Parkin as well as wild-type PINK1, whereas recruitment of Parkin to the mitochondria by the 1602-insert mutant was abolished (Fig. 5, B–D), suggesting that the pathology of this PINK1 mutation is mislocalization and consequent inactivation of Parkin.

Mitochondrial localization and kinase activity of PINK1 are essential for translocation of Parkin to damaged mitochondria

Finally, we investigated the role of various PINK1 domains (Fig. 5 A) in the mitochondrial recruitment of Parkin. PINK1 is composed of an atypical N-terminal mitochondrial localization signal and transmembrane domain, a kinase domain in the middle, and a conserved C-terminal domain (Zhou et al., 2008). Deletion of the N-terminal 91 aa abolished the mitochondrial localization of PINK1 (Zhou et al., 2008). We also confirmed that the ΔN91 and ΔN155 mutants did not target to the mitochondria even after CCCP treatment (Fig. S3). We also generated a mutant containing the triple K219A, D362A, and D384A mutations that abolish kinase activity (Beilina et al., 2005) and a C-terminal domain deletion mutant associated with PINK1 dysfunction (Sim et al., 2006; Yang et al., 2006). The kinase-dead and ΔC72 mutants of PINK1 colocalized with damaged mitochondria similar to wild type (Fig. S3). When introduced into *PINK1*$^{-/-}$ cells harboring GFP-Parkin, the mutants were unable to complement the mislocalization and inactivation of Parkin (Fig. 5, B–D), even though the mutant PINK1 proteins were expressed (Fig. 5 D and Fig. S3). These results indicate that the kinase activity and mitochondrial targeting of PINK1 are essential for the mitochondrial recruitment of Parkin.

Conclusion

In summary, we have shown that (a) PINK1 is a Parkin-recruitment factor that recruits Parkin from the cytoplasm to damaged mitochondria in a membrane potential–dependent manner for mitochondrial degradation, (b) endogenous PINK1 is constitutively degraded at the mitochondria, but its localization is specifically linked to a decrease in membrane potential, (c) under steady-state conditions, the E3 activity of Parkin is repressed in the cytoplasm but is liberated by PINK1-dependent mitochondrial localization, and (d) the aforementioned phenomena are presumably etiologically important in part because they were impeded for the most part by disease-linked mutations of PINK1 or Parkin. We believe that these results provide solid insight into the molecular mechanisms of PD pathogenesis not only for familial forms caused by *Parkin* and *PINK1* mutations but also major sporadic forms of PD.

Materials and methods

Cell culture and transfection

MEFs derived from embryonic day 12.5 embryos of PINK1 knockout mice (provided by J. Shen, Harvard Medical School, Boston, MA) were mechanically dispersed by repeated passage through a P1000 pipette tip and plated with MEF media containing DME, 10% FCS, β-mercaptoethanol (Sigma-Aldrich), 1× nonessential amino acids, and 1 mM L-glutamine. Various stable transformants of MEFs were established by infecting MEFs with recombinant retroviruses. HA-Parkin, GFP-Parkin, PINK1 (provided by Y. Nakamura, T. Iwatsubo, and S. Takatori, University of Tokyo, Bunkyo-ku, Tokyo, Japan), or various PINK1 mutants were cloned into a pMXs-puro vector. Retrovirus packaging cells, PLAT-E (provided by T. Kitamura, University of Tokyo; Kitamura et al., 2003), were transfected with the aforementioned vectors and were cultured at 37°C for 24 h. After changing the medium, cells were further incubated at 37°C for 24 h, and the viral supernatant was collected and used for infection. MEFs were plated on 35-mm dishes at 24 h before infection, and the medium was replaced with the aforementioned undiluted viral supernatant with 8 μg/ml polybrene (Sigma-Aldrich). 2 d later, transformants were selected by the medium containing 10 μg/ml puromycin.

Cell fractionation and immunoprecipitation

To depolarize the mitochondria, HeLa and SH-SY5Y cells were treated with 10 μM CCCP, and MEFs were treated with 30 μM CCCP. For fractionation experiments, HeLa and SH-SY5Y cells were treated with CCCP for 1–5 h and subsequently treated with 1 mM DSP (Thermo Fisher Scientific) in PBS for 1 h on ice, inactivated by 10 mM glycine in PBS three times, and suspended in chappell-perry buffer (0.15 M KCl, 20 mM Hepes-NaOH, pH 8.1, 5 mM $MgCl_2$, and protease and phosphatase inhibitor [Roche]). Cells were disrupted by five passages through a 25-gauge needle (with 1-ml syringe), debris was removed by centrifugation at 1,000 *g* for 7 min, and the supernatant was subjected to 10,000 *g* for 10 min to separate the mitochondria-rich fraction from the cytosol-rich fraction. Immunoblotting and immunoprecipitation were performed by conventional methods. To detect the ubiquitylation of GFP-Parkin, the cell lysate of HeLa cells (10 μM CCCP for 1 h) or MEFs (30 μM CCCP for 3 h) was collected in the presence of 10 mM *N*-ethylmaleimide to protect ubiquitylated Parkin from deubiquitylation enzymes. To monitor the degradation of endogenous PINK1, HeLa cells were treated with 10 μM CCCP and 50 μg/ml cycloheximide as depicted in Fig. 3 G and were subjected to immunoblotting.

Immunocytochemistry

To depolarize the mitochondria, HeLa cells (provided by A. Tanaka and R. Youle, National Institutes of Health, Bethesda, MD) were treated with 10 μM CCCP for 1 h (exogenous Parkin and PINK1) or 5 h (endogenous PINK1), and MEFs were treated with 30 μM CCCP for 3–4 h (Figs. 4 A and 5 B; and Fig. S3 B) or 24 h (Fig. 4 D and Fig. S2 A). For immunofluorescence experiments, cells were fixed with 4% paraformaldehyde, permeabilized with 50 μg/ml digitonin, and stained with primary antibodies described in the next section and with the following secondary antibodies: mouse and/or rabbit Alexa Fluor 488, 568, and 647 (Invitrogen). N-terminal 34 aa of PINK1 were fused to GFP to stain mitochondria in the triple staining experiments. To monitor the mitochondrial membrane potential, MEFs were treated with 50 nM MitoTracker red CMXRos (Invitrogen) for 15 min, washed three times, and incubated for an additional 10 min before fixation, as reported previously (Narendra et al., 2008). Cells were imaged using a laser-scanning microscope (LSM510 META; Carl Zeiss, Inc.) with a Plan-Apochromat 63× NA 1.4 oil differential interference contrast objective lens. Image contrast and brightness were adjusted in Photoshop (Adobe).

Downloaded from jcb.rupress.org on May 26, 2011

Published April 19, 2010

Antibodies

Antibodies used in this study are as follows: antiactin (AC-40; Sigma-Aldrich), anti–cytochrome *c* (6H2.B4; BD), anti-Flag (M2; Sigma-Aldrich), anti-GFP (3E6 [Wako Chemicals USA, Inc.]; or A6455 [Invitrogen]), anti-HA (12CA5; Roche), anti-Hsp70 (MBL), anti–lactate dehydrogenase (Abcam), anti-Parkin (#2132 [Cell Signaling Technology] for immunocytochemistry; or PRK8 [Sigma-Aldrich] for immunoblotting), anti-PINK1 (Novus), anti-Tom20 (FL-145 and F-10; Santa Cruz Biotechnology, Inc.), antiubiquitin (P4D1 [Santa Cruz Biotechnology, Inc.]; or FK2 [MBL]), and anti-V5 (Invitrogen).

Online supplemental material

Fig. S1 shows various control experiments for immunoblotting and immunocytochemistry. Fig. S2 shows that Parkin promoted degradation of depolarized mitochondria via autophagy. Fig. S3 shows the subcellular localization of pathogenic and deletion mutants of PINK1 after CCCP treatment. Online supplemental material is available at http://www.jcb.org/cgi/content/full/jcb.200910140/DC1.

We thank Dr. T. Kitamura for providing the PLAT-E cells, Drs. A. Tanaka and R. Youle for NIH HeLa cells, Dr. J. Shen for *PINK1* knockout MEFs, and Drs. Y. Nakamura, T. Iwatsubo, and S. Takatori for plasmids.

This work was supported by Grants-in-Aid for Young Scientist (B) (to N. Matsuda, K. Shiba, and S. Saiki) and by Specially Promoted Research (to K. Tanaka) from the Ministry of Education, Culture, Sports, Science and Technology of Japan and Heath and Labor Science Research grants (to N. Hattori and K. Tanaka).

Note added in review. While our manuscript was under review, Geisler et al. (2010), Narendra et al. (2010), and Vives-Bauza et al. (2010) independently published results that are consistent with those described herein.

Submitted: 26 October 2009
Accepted: 22 March 2010

References

Beilina, A., M. Van Der Brug, R. Ahmad, S. Kesavapany, D.W. Miller, G.A. Petsko, and M.R. Cookson. 2005. Mutations in PTEN-induced putative kinase 1 associated with recessive parkinsonism have differential effects on protein stability. *Proc. Natl. Acad. Sci. USA*. 102:5703–5708. doi:10.1073/pnas.0500617102

Clark, I.E., M.W. Dodson, C. Jiang, J.H. Cao, J.R. Huh, J.H. Seol, S.J. Yoo, B.A. Hay, and M. Guo. 2006. *Drosophila* pink1 is required for mitochondrial function and interacts genetically with parkin. *Nature*. 441: 1162–1166. doi:10.1038/nature04779

Denison, S.R., F. Wang, N.A. Becker, B. Schüle, N. Kock, L.A. Phillips, C. Klein, and D.I. Smith. 2003. Alterations in the common fragile site gene Parkin in ovarian and other cancers. *Oncogene*. 22:8370–8378. doi:10.1038/sj.onc.1207072

Dodson, M.W., and M. Guo. 2007. Pink1, Parkin, DJ-1 and mitochondrial dysfunction in Parkinson's disease. *Curr. Opin. Neurobiol.* 17:331–337. doi:10.1016/j.conb.2007.04.010

Exner, N., B. Treske, D. Paquet, K. Holmström, C. Schiesling, S. Gispert, I. Carballo-Carbajal, D. Berg, H.H. Hoepken, T. Gasser, et al. 2007. Loss-of-function of human PINK1 results in mitochondrial pathology and can be rescued by parkin. *J. Neurosci.* 27:12413–12418. doi:10.1523/JNEUROSCI.0719-07.2007

Gautier, C.A., T. Kitada, and J. Shen. 2008. Loss of PINK1 causes mitochondrial functional defects and increased sensitivity to oxidative stress. *Proc. Natl. Acad. Sci. USA*. 105:11364–11369. doi:10.1073/pnas.0802076105

Geisler, S., K.M. Holmström, D. Skujat, F.C. Fiesel, O.C. Rothfuss, P.J. Kahle, and W. Springer. 2010. PINK1/Parkin-mediated mitophagy is dependent on VDAC1 and p62/SQSTM1. *Nat. Cell Biol.* 12:119–131. doi:10.1038/ncb2012

Hampe, C., H. Ardila-Osorio, M. Fournier, A. Brice, and O. Corti. 2006. Biochemical analysis of Parkinson's disease-causing variants of Parkin, an E3 ubiquitin-protein ligase with monoubiquitylation capacity. *Hum. Mol. Genet.* 15:2059–2075. doi:10.1093/hmg/ddl131

Hardy, J., H. Cai, M.R. Cookson, K. Gwinn-Hardy, and A. Singleton. 2006. Genetics of Parkinson's disease and parkinsonism. *Ann. Neurol.* 60:389–398. doi:10.1002/ana.21022

Hristova, V.A., S.A. Beasley, R.J. Rylett, and G.S. Shaw. 2009. Identification of a novel Zn2+-binding domain in the autosomal recessive juvenile Parkinson-related E3 ligase parkin. *J. Biol. Chem.* 284:14978–14986. doi:10.1074/jbc.M808700200

Imai, Y., M. Soda, and R. Takahashi. 2000. Parkin suppresses unfolded protein stress-induced cell death through its E3 ubiquitin-protein ligase activity. *J. Biol. Chem.* 275:35661–35664. doi:10.1074/jbc.C000447200

Kitada, T., S. Asakawa, N. Hattori, H. Matsumine, Y. Yamamura, S. Minoshima, M. Yokochi, Y. Mizuno, and N. Shimizu. 1998. Mutations in the parkin gene cause autosomal recessive juvenile parkinsonism. *Nature*. 392:605–608. doi:10.1038/33416

Kitamura, T., Y. Koshino, F. Shibata, T. Oki, H. Nakajima, T. Nosaka, and H. Kumagai. 2003. Retrovirus-mediated gene transfer and expression cloning: powerful tools in functional genomics. *Exp. Hematol.* 31:1007–1014.

Komatsu, M., S. Waguri, T. Ueno, J. Iwata, S. Murata, I. Tanida, J. Ezaki, N. Mizushima, Y. Ohsumi, Y. Uchiyama, et al. 2005. Impairment of starvation-induced and constitutive autophagy in Atg7-deficient mice. *J. Cell Biol.* 169:425–434. doi:10.1083/jcb.200412022

Lim, K.L. 2007. Ubiquitin-proteasome system dysfunction in Parkinson's disease: current evidence and controversies. *Expert Rev. Proteomics*. 4:769–781. doi:10.1586/14789450.4.6.769

Matsuda, N., and K. Tanaka. 2010. Does impairment of the ubiquitin-proteasome system or the autophagy-lysosome pathway predispose individuals to neurodegenerative disorders such as Parkinson's disease? *J. Alzheimers Dis.* 19:1–9.

Matsuda, N., T. Kitami, T. Suzuki, Y. Mizuno, N. Hattori, and K. Tanaka. 2006. Diverse effects of pathogenic mutations of Parkin that catalyze multiple monoubiquitylation in vitro. *J. Biol. Chem.* 281:3204–3209. doi:10.1074/jbc.M510393200

Moore, D.J., A.B. West, V.L. Dawson, and T.M. Dawson. 2005. Molecular pathophysiology of Parkinson's disease. *Annu. Rev. Neurosci.* 28:57–87. doi:10.1146/annurev.neuro.28.061604.135718

Narendra, D., A. Tanaka, D.F. Suen, and R.J. Youle. 2008. Parkin is recruited selectively to impaired mitochondria and promotes their autophagy. *J. Cell Biol.* 183:795–803. doi:10.1083/jcb.200809125

Narendra, D.P., S.M. Jin, A. Tanaka, D.F. Suen, C.A. Gautier, J. Shen, M.R. Cookson, and R.J. Youle. 2010. PINK1 is selectively stabilized on impaired mitochondria to activate Parkin. *PLoS Biol.* 8:e1000298. doi:10.1371/journal.pbio.1000298

Park, J., S.B. Lee, S. Lee, Y. Kim, S. Song, S. Kim, E. Bae, J. Kim, M. Shong, J.M. Kim, and J. Chung. 2006. Mitochondrial dysfunction in *Drosophila* PINK1 mutants is complemented by parkin. *Nature*. 441:1157–1161. doi:10.1038/nature04788

Pawlyk, A.C., B.I. Giasson, D.M. Sampathu, F.A. Perez, K.L. Lim, V.L. Dawson, T.M. Dawson, R.D. Palmiter, J.Q. Trojanowski, and V.M. Lee. 2003. Novel monoclonal antibodies demonstrate biochemical variation of brain parkin with age. *J. Biol. Chem.* 278:48120–48128. doi:10.1074/jbc.M306889200

Schapira, A.H. 2008. Mitochondria in the aetiology and pathogenesis of Parkinson's disease. *Lancet Neurol.* 7:97–109. doi:10.1016/S1474-4422(07)70327-7

Shimura, H., N. Hattori, S. Kubo, Y. Mizuno, S. Asakawa, S. Minoshima, N. Shimizu, K. Iwai, T. Chiba, K. Tanaka, and T. Suzuki. 2000. Familial Parkinson disease gene product, parkin, is a ubiquitin-protein ligase. *Nat. Genet.* 25:302–305. doi:10.1038/77060

Silvestri, L., V. Caputo, E. Bellacchio, L. Atorino, B. Dallapiccola, E.M. Valente, and G. Casari. 2005. Mitochondrial import and enzymatic activity of PINK1 mutants associated to recessive parkinsonism. *Hum. Mol. Genet.* 14:3477–3492. doi:10.1093/hmg/ddi377

Sim, C.H., D.S. Lio, S.S. Mok, C.L. Masters, A.F. Hill, J.G. Culvenor, and H.C. Cheng. 2006. C-terminal truncation and Parkinson's disease-associated mutations down-regulate the protein serine/threonine kinase activity of PTEN-induced kinase-1. *Hum. Mol. Genet.* 15:3251–3262. doi:10.1093/hmg/ddl398

Takatori, S., G. Ito, and T. Iwatsubo. 2008. Cytoplasmic localization and proteasomal degradation of N-terminally cleaved form of PINK1. *Neurosci. Lett.* 430:13–17. doi:10.1016/j.neulet.2007.10.019

Valente, E.M., P.M. Abou-Sleiman, V. Caputo, M.M. Muqit, K. Harvey, S. Gispert, Z. Ali, D. Del Turco, A.R. Bentivoglio, D.G. Healy, et al. 2004. Hereditary early-onset Parkinson's disease caused by mutations in PINK1. *Science*. 304:1158–1160. doi:10.1126/science.1096284

Vives-Bauza, C., C. Zhou, Y. Huang, M. Cui, R.L. de Vries, J. Kim, J. May, M.A. Tocilescu, W. Liu, H.S. Ko, et al. 2010. PINK1-dependent recruitment of Parkin to mitochondria in mitophagy. *Proc. Natl. Acad. Sci. USA*. 107:378–383. doi:10.1073/pnas.0911187107

Yang, Y., S. Gehrke, Y. Imai, Z. Huang, Y. Ouyang, J.W. Wang, L. Yang, M.F. Beal, H. Vogel, and B. Lu. 2006. Mitochondrial pathology and muscle and dopaminergic neuron degeneration caused by inactivation of *Drosophila* Pink1 is rescued by Parkin. *Proc. Natl. Acad. Sci. USA*. 103:10793–10798. doi:10.1073/pnas.0602493103

Downloaded from jcb.rupress.org on May 26, 2011

Published April 19, 2010

Zhang, Y., J. Gao, K.K. Chung, H. Huang, V.L. Dawson, and T.M. Dawson. 2000. Parkin functions as an E2-dependent ubiquitin- protein ligase and promotes the degradation of the synaptic vesicle-associated protein, CDCrel-1. *Proc. Natl. Acad. Sci. USA*. 97:13354–13359. doi:10.1073/pnas.240347797

Zhou, C., Y. Huang, Y. Shao, J. May, D. Prou, C. Perier, W. Dauer, E.A. Schon, and S. Przedborski. 2008. The kinase domain of mitochondrial PINK1 faces the cytoplasm. *Proc. Natl. Acad. Sci. USA*. 105:12022–12027. doi:10.1073/pnas.0802814105

Downloaded from jcb.rupress.org on May 26, 2011